A Double-Point Mutation in the Selectivity Filter Site of the KCNQ1 Potassium Channel Results in a Severe Phenotype, LQT1, of Long QT Syndrome

TARUNA IKRAR, M.D.,* HARUO HANAWA, M.D., PH.D.,* HIROSHI WATANABE, M.D., PH.D.,*,† SHINSUKE OKADA, M.D.,* YOSHIYASU AIZAWA, M.D., PH.D.,*,‡ MAHMOUD M. RAMADAN, M.D.,* SATORU KOMURA, M.D.,* FUMIO YAMASHITA, M.D., PH.D.,* MASAOMI CHINUSHI, M.D., PH.D.,* and YOSHIFUSA AIZAWA, M.D., P.H.D.*

From the *Division of Cardiology, First Department of Internal Medicine, Niigata University Graduate School of Medical and Dental Sciences, Niigata, Japan; †Division of Clinical Pharmacology, Vanderbilt University School of Medicine, Nashville, Tennessee, USA; and ‡Masonic Medical Research Laboratory, Utica, New York, USA

Mutation in the Selectivity Filter of the KCNQ1. ***Introduction:*** **Slowly activating delayed-rectifier potassium currents in the heart are produced by a complex protein with α and β subunits composed of the potassium voltage-gated channel KQT-like subfamily, member 1 (KCNQ1) and the potassium voltage-gated channel Isk-related family, member 1 (KCNE1), respectively. Mutations in KCNQ1 underlie the most common type of hereditary long QT syndrome (LQTS). Like other potassium channels, KCNQ1 has six transmembrane domains and a highly conserved potassium selectivity filter in the pore helix called "the signature sequence." We aimed to investigate the functional consequences of a newly identified mutation within the signature sequence.**

Methods and Results: **Potassium channel genomic DNA from a family with clinical evidence of LQTS was amplified by polymerase chain reaction (PCR), and the resulting products were then sequenced. Three family members had a double-point mutation in KCNQ1 at nucleotides 938 (T-to-A) and 939 (C-to-A), resulting in an isoleucine-to-lysine change at amino acid position 313. These patients displayed prolonged QTc intervals (629, 508, and 500 $ms^{1/2}$, respectively) and repetitive episodes of syncope, but no deafness. Three-dimensional structure modeling of KCNQ1 revealed that this mutation is located at the center of the channel pore. COS-7 cells displayed a lack of current when transfected with a plasmid expressing the mutant. In addition, the mutant displayed a dominant negative effect on current but appeared normal with respect to plasma membrane integration.**

Conclusion: **An I313K mutation within the selectivity filter of KCNQ1 results in a dominant-negative loss of channel function, leading to a long QT interval and subsequent syncope.** *(J Cardiovasc Electrophysiol, Vol. 19, pp. 541-549, May 2008.)*

arrhythmia, long QT syndrome, potassium channel, KCNQ1, selectivity filter

Introduction

Long QT syndrome (LQTS) is a cardiac disorder characterized by a prolonged QT interval, which predisposes the patient to syncope and sudden arrhythmic death.[1] Most commonly, a prolonged QT interval results from reductions in either the rapidly (IKr) or the slowly (IKs) activating delayed rectifier K^+ current.[2] The inherent instability of cardiac repolarization is accentuated by a prolonged action potential and leads to the development of early after-depolarization, the trigger for torsade de pointes.[3]

KCNQ1 (also known as KVLQT1) is the voltage-gated K^+ channel α-subunit that forms a tetrameric complex in the plasma membrane and selectively conducts K^+ ions (Fig. 1, supplementary online). Although homomeric KCNQ1 channels are functional, it has become increasingly evident that at least some of the physiological functions of KCNQ1 require its coassembly with a single transmembrane domain ancillary subunit minK (known as KCNE1) to form the cardiac IKs.[4] Mutation of KCNQ1 can lead to dysfunction of this channel, causing cardiac LQTS, with serious subsequent arrhythmias such as ventricular fibrillation and cardiac arrest.[5] KCNQ1 comprises six transmembrane domains (S1–S6), including a voltage sensor (S4) and a pore helix selectivity filter segment (P-loop) that connects S5 and S6. The selectivity filter is defined by a highly conserved amino acid sequence motif (TIGYG), as seen in the bacterial KcsA channel,[6,7] and is the central structural element that defines K^+ channels.[6,8]

We recently reported an I313K mutation at the selectivity filter site (i.e., the mutant motif is TKGYG) in a female patient with LQTS and presented her clinical characteristics.[9] However, the molecular bases underlying that mutation were not identified. In the present work, we investigate the functional consequences of the mutant K^+ channel and examine its structure in detail.

This work was supported by grants from the Japanese Ministry of Education, Science and Culture, Tokyo, Japan.

Address for correspondence: Yoshifusa Aizawa, M.D., Ph.D., First Department of Internal Medicine, 1-754 Asahimachi Dori, Niigata 951-8510, Japan. Fax: +81-25-228-5611; E-mail: aizaways@med.niigata-u.ac.jp

Manuscript Received 13 July 2007; Revised manuscript received 19 November 2007; Accepted for publication 21 November 2007.

doi: 10.1111/j.1540-8167.2007.01076.x

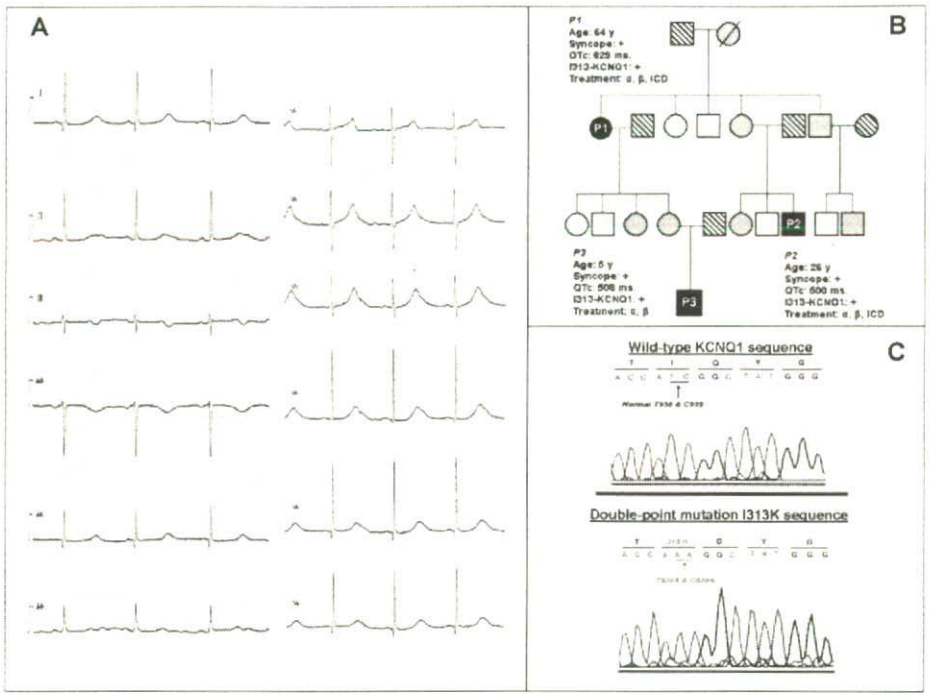

Figure 1. *A: Transthoracic 12-lead ECG obtained from the affected proband (P1), a 64-year-old Japanese woman from a family with a compound I313K mutation in KCNQ1. B: The pedigree of a family with I313K mutation. Individuals are assigned as males (squares) or females (circles); affected (black) or unaffected (white); reported long QT (LQT) phenotype (gray) or unreported (slashes). The "affected" individuals are the only ones that have presented with syncope and received medical treatment for the syndrome. Both "unaffected" and "unreported" individuals are phenotypically normal, with the "unaffected" individuals having been genetically or clinically examined for long QT syndrome (LQTS) and the "unreported" individuals remaining unexamined. The following information is indicated for the three probands (P1, P2, and P3): QTc = heart rate-corrected QT interval; I313K-KCNQ1= isoleucine-to-lysine substitution in the KCNQ1 protein; ICD= implantable cardiovascular defibrillator; β = β-adrenergic receptor blocker treatment; α= α-adrenergic receptor blocker treatment. C: Coding region sequence around the KCNQ1 double-point mutation from genomic DNA isolated from the three probands. The arrow denotes the double-point mutation (T-to-A translation at position 938 and C-to-A translation at position 939 of the KCNQ1 cDNA sequence). Amino acid residues are listed above their corresponding nucleotide codons. The double-point mutation results in the substitution of isoleucine with lysine at amino acid position 313 (I313K) in the KCNQ1 selectivity filter sequence.*

Subjects and Methods

Patients

Three Japanese patients from the same family with a KCNQ1 mutation—who were referred to Niigata University Hospital (Niigata City, Japan) for molecular/genetic workup for LQTS—were selected for careful clinical and electrophysiological analysis. Clinical evaluation included a full medical history (including family history), thorough clinical examination, 12-lead exercise electrocardiogram (ECG), and ambulatory ECG monitoring whenever possible. The QT interval was calculated and corrected by Bazett's formula to identify a prolonged QT or QTc interval.

All subjects or their guardians gave informed consent for the genetic and clinical studies. This study was approved by the ethics committee of Niigata University Graduate School of Medicine.

Gene Isolation and Mutation Analysis

Genomic DNA was extracted from whole blood using a Sepa Gene reagent set (Sankou Junyaku, Co., Tokyo, Japan) and isolated from leukocyte nuclei by conventional methods.[10,11] The genes of interest were amplified from genomic DNA by standard polymerase chain reaction (PCR), and products were sequenced in both directions using the same primers utilized for PCR as follows: 3′-CTCTTTTCTGAGACGGAGATGAAC (for 3′-KvLQT1-1739) and 5′-TCTACAACTTCCTCGAGCGTC (for 5′-KvLQT1-329). The first primer listed was used to sequence in the reverse direction beginning at nucleotide position 1739 and the second primer listed was used to sequence in the forward direction beginning at nucleotide position 329. DNA sequencing was performed by the dideoxynucleotide chain termination method with fluorescent dideoxynucleotides using a DNA sequencer (ABI PRISM 310 Genetic analyzer, Perkin Elmer Applied Biosystems, CA, USA) and the Big Dye terminator premix reagent V1.1 (Applied Biosystems). For genetic screening, a direct DNA sequencing method was used for KCNE2,[11] KCNJ2,[12] KCNQ1, KCNH2, SCN5A, and KCNE1.[13] Electropherograms from patients with mutant KCNQ1 were compared with those from control subjects having a wild-type (WT) KCNQ1 sequence.[10,11,14,15]

Construction of Plasmid DNA for Gene Transfer

For patch-clamping experiments, two types of plasmids were needed. First, the plasmid vector pIRES2-EGFP, into which WT-KCNQ1 was already inserted using *Nhe* I and *Bam* HI restriction sites (making the pIRES2-EGFP-KCNQ1 plasmid as described previously[11]), was a gift from Dr. M. Horie (Kyoto University, Kyoto, Japan). Second, we prepared the

plasmid vector for mutant KCNQ1 (pIRES2-EGFP-I313K) according to the following steps. An initial PCR product was amplified from the pIRES2-EGFP-KCNQ1 template using KOD Plus DNA polymerase (TOYOBO, Osaka, Japan) and the primer sets (5′-CCATTTCCATCATCGACCTCA-3′ and 5′-TCTGGGGCACCTTGTCCCCATAGCCttTGGTGGTG-ACTGTGACCACCCCCCA-3′) and (5′-TGGGGGGtGGT-CACACCACCAaaGGCTATGGGGACAAGGTGCCCCA-GA-3′ and 5′-AAGGAGAGCAGCTGGTGAAG-3′) (*lower case letters indicate mutation sites*). The resulting product was again amplified by PCR using the primers (5′-CCATTTCCATCATCGACCTCA-3′ and 5′-AAGGAGAG-CGCTGGTGAAG-3′). This final PCR product was ligated to the pIRES2-EGFP WT-KCNQ1 vector using the *Pst* I sites at nucleotide positions 697 and 1675 of KCNQ1. The PCR insert was also cleaved with *Pst* I prior to ligation. For the aim of confocal microscopic study, two types of plasmids were also required. First, the plasmid vector pEGFP-N1-KCNQ1 that was prepared by inserting the *Nhe* I/*Bam* HI fragment from pIRES2-EGFP-KCNQ1 (containing WT-KCNQ1) into the *Nhe* I and *Bam* HI sites of the pEGFP-N1 vector as described previously.[12] Second, the plasmid pEGFP-N1-I313K was prepared by inserting the *Nhe* I/*Bam* HI fragment from pIRES2-EGFP-I313K (containing the mutant KCNQ1) into the *Nhe* I and *Bam* HI sites of the pEGFP-N1 vector. The resulting cloned plasmids were then transformed into *Escherichia coli* JM109 competent cells and purified using a Quantum Prep Plasmid Maxi prep kit (Bio-Rad Laboratories, Hercules, CA, USA). WT-KCNQ1 was amplified from genomic DNA using the 14 PCR primer sets shown in Table 1. These primers were used to obtain the full-length gene from the genomic DNA and the resulting PCR products were then combined together to create the complete WT-KCNQ1 expression plasmid.

Culture and Transfection of COS-7 Cells

The COS-7 monkey kidney cell line was obtained from the American Type Cell Collection and cultured in Dulbecco's Modified Eagles Medium (Invitrogen Corporation, Gibco-BRL, Rockville, MD, USA) supplemented with 1% penicillin-streptomycin (prepared with 10,000 units/mL penicillin G sodium and 10,000 μg/mL streptomycin sulfate in 0.85% saline) and 10% fetal bovine serum in a humidified 5% CO_2 incubator at 37°C.[10,11] The number of cells seeded per milliliter of medium was 2×10^5 on average. Cultured cells were seeded in 60-mm plates 24 hours before transfection, then transiently transfected with various plasmids by the Fugene-6 method (Roche Applied Science, Indianapolis, IN, USA). Because COS-7 cells are devoid of endogenous KCNQ1 or KCNE1, they are considered an excellent system for examination of exogenous expression of these proteins.

In the electrophysiological experiments, 1.0 μg or 0.5 μg of pIRES2-EGFP-KCNQ1, 1.0 μg of pIRES2-EGFP-I313K, or 0.5 μg pIRES2-EGFP-KCNQ1 + 0.5 μg pIRES2-EGFP-I313K were used in combination with an equivalent amount of KCNE1 or in its absence.[11]

Electrophysiological Experiments

The whole-cell patch-clamp method was applied to COS-7 cells transfected with pIRES2-EGFP-KCNQ1 (WT) and/or pIRES2-EGFP-I313K (mutant) plasmids as described.[10,12,16] In brief, cells were allowed to settle on the bottom of a bath (0.5 mL) mounted on an inverted microscope (Olympus Corp, Tokyo, Japan). Cells were superfused with the bath solution (140 mmol NaCl, 5.4 mmol KCl, 0.5 mmol $MgCl_2$, 1.8 mmol $CaCl_2$, 0.33 mmol NaH_2PO_4, 5.5 mmol glucose, and 5 mmol HEPES [pH 7.4 adjusted with NaOH]). When inserted into the cell/bath solution, a glass pipette with an internal diameter of 1.0–1.5 μm had a resistance of 4–6 MΩ when filled with the following internal solution: 100 mmol/L K-aspartate, 20 mmol/L KCl, 5 mmol/L ATP-Mg, 5 mmol/L phosphocreatine-dipotassium, 5 mmol/L EGTA, 5 mmol/L HEPES, and 1 mmol/L $CaCl_2$ (pH 7.2 adjusted with KOH).

A patch-clamp amplifier (Axopatch 200B, Axon Instruments, CA, USA) was used to record membrane currents. After forming a whole-cell configuration, cell membrane capacitance was estimated by analyzing the transient capacitance elicited by 5-mV hyperpolarizing pulses.[10,11,17] A series resistance compensation of 50–70% was built into the amplifier's circuit. Cells were held at a potential of −80 mV and depolarizing pulses of various potentials ranging from −80 mV to +80 mV in 20 mV increments for 2 seconds were applied followed by repolarization to −40 mV for 2 seconds to record tail currents.[15] Software (pCLAMP 8.0, Axon Instruments) was used to generate the pulse protocol, data acquisition, and analysis. All experiments were conducted at room temperature.

TABLE 1

Forward and Reverse Primers Used to Amplify KCNQ1

Primer set	Forward	Reverse
1	5′-AGATTAGGGGAATTTTACAGCTTG-3′	5′-TTCTCTGATACTGAAATGAGTGCC-3′
2	5′-GAGAGCAGGGTGTATGCTCTTC-3′	5′-CCCAGCACATGGCTCAGT-3′
3	5′-TGGACATATACCCAGCCTCC-3′	5′-CAGCTCAGAGGAAGGTGAGC-3′
4	5′-GAGTTGTGAGGAGTGGGCTATATT-3′	5′-CCGAAGTCTCAAGACACCAGT-3′
5	5′-AGAGTGGTGGGTTTGGGTTAG-3′	5′-CTTGGTTCTGAACGTAAGTGGGT-3′
6	5′-TGGCCTGTGGACGGGA-3′	5′-CAGTGACCAAAATGACAGTGA-3′
7	5′-AGCTGTAGCTTCATAAGGGC-3′	5′-ACAGGCTGTACCAAGCCAAAT-3′
8	5′-GTCCCTGTCCGGGTTATGT-3′	5′-AAGGGAGAAACTCACTGGCTT-3′
9	5′-ACAAGCTCCACTCCTCACCTG-3′	5′-CTAGGCGAGTAGATAGCACTCTGG-3′
10	5′-GAACACTCTCCTTGTTTCTGAAG-3′	5′-TAGGCACTGCAGGTCTCAGATAG-3′
11	5′-GAGCTCCCAGGTCTTCACAAG-3′	5′-AGAGGCAAGAACTCAGGGTCGC-3′
12	5′-GTCAAGCTGTCTGTCCCACA-3′	5′-CTAAAACGTACTTTGGAGCCACTT-3′
13	5′-CACCCCTGGTATTTTTGTCATAG-3′	5′-CTTCACGTTCACACGCAGAC-3′
14	5′-CCACCACTGACTCTCTCGTCT-3′	5′-AGAGTGGGGCTCTTCTCTCTG-3′

About 5% of COS-7 cells transfected with WT-KCNQ1 plasmid failed to elicit WT current. The reason for this failure may have been a leak of current or possible cell damage. In addition, to be confident of the currents obtained from the remaining cells, our analyses only included recordings obtained by Giga-seal after applying the following quality control criteria[18] for the patch-clamp technique: (1) the starting seal resistance was required to be better than 1 GΩ; (2) the series resistance was required to be lower than 20 MΩ throughout the recording; (3) the membrane potential was required to be more negative than –50 mV if the normal high-potassium intracellular solution was used; and (4) cell capacitance and resistance were required to be stable. Furthermore, to check the quality of our findings, COS-7 cells transfected with WT-KCNQ1 were compared with the results of Barhanin *et al.*[19] and Sanguinetti *et al.*,[20] regarding the properties and biophysical characteristics of the WT-KCNQ1 potassium current. Our results were indeed close to those presented in these two reports, indicating the high quality and accuracy of our findings.

Confocal Imaging

The yellow fluorescent protein (YFP)-tagged pEGFP-N1-KCNQ1 and the cyan fluorescent protein (CFP)-tagged pEGFP-N1-I313K expression vectors were transfected into COS-7 cells in glass-bottomed well slides (Matsunami Glass IND, Tokyo, Japan). At 48 hours posttransfection, cells were fixed on a glass slide with 4% paraformaldehyde.

Some experiments required that a portion of the COS-7 cells be stripped (with 0.25% trypsin for 60 seconds) from the cover slip after paraformaldehyde treatment so that the total cell surface on the slide was reduced. In addition, the COS-7 cells remaining on the cover slip were then suspended in normal Tyrode's solution. Cells were visualized using an FV500 confocal laser scanning microscope (Olympus Corp). An Argon laser was used to excite the YFP (excitation wavelength = 514 nm) and CFP (excitation wavelength = 458 nm).[21] YFP fluorescence was detected with a BP535/536 filter and assigned as yellow, whereas CFP fluorescence was detected with a BP465/495 filter and assigned as blue. Merged images were obtained by overlaying images from the individual channels using the confocal laser scanning microscope and were assigned as white. Confocal microscopy experiments were performed on the same day for both groups of COS-7 cells transfected with pEGFP-N1-KCNQ1 and pEGFP-N1-I313K plasmids, with identical parameters used for all manipulations.[10] A three-dimensional model of the S5 to S6 domains of the KCNQ1 subunit was constructed based on homology with the crystal structure of the corresponding domains of KcsA, a proton-activated K^+ channel isolated from *Streptomyces lividans*.[7]

Statistical Analysis

Data analyses were performed with SPSS for Windows ver.13 (SPSS Inc., Chicago, IL USA). Normality of distribution of the values of different variables was assessed by the 1-sample Kolmogorov-Smirnov test. Results for continuous normal data were expressed as mean ± standard error of mean. The comparison of means of continuous normal variables across a grouping variable with two levels was done by the Student's *t*-test and the comparison of means of continuous normal variables across a grouping variable with several levels was done by one-way analysis of variance (ANOVA). A two-sided significance level of 0.05 was used for all analyses.

Results

Clinical and Genetic Phenotypes

A 64-year-old female was referred for genetic evaluation of LQTS (Fig. 1A, proband P1). She reported having syncope since the age of 34 years, but had no family history of sudden cardiac death. She had been treated with β- and α-adrenergic receptor blockers, and finally with an implantable cardioverter defibrillator (ICD). She had four children, the youngest being 26-year-old twins, both of whom were diagnosed with long QT syndrome type 1 (LQT1). One of the twins had one male child aged 5 years (proband P3) who was also diagnosed with LQT1 and was receiving β- and α-adrenergic receptor blockers. Another proband (P2) experienced syncope for the first time at the age of 3 years and had been treated with β- and α-adrenergic receptor blockers and an ICD (Fig. 1B). All patients were diagnosed as LQT1 by the present study except proband P1, who was previously diagnosed.[9] Notably, the three probands had no deafness. All three probands were found to have a double-point mutation at nucleotide positions 938 (T-to-A) and 939 (C-to-A) in the KCNQ1 gene. The mutations resulted in an isoleucine-to-lysine substitution at amino acid residue 313 of KCNQ1, situated at the selectivity filter of the KCNQ1 channel (Fig. 1C). These two nucleotide substitutions were not observed in blood samples of more than 100 unrelated ethnically matched healthy individuals (data not shown). Also, none of the mutations previously identified among other long QT-related genes (KCNH2, KCNE1, KCNE2, SCN5A, and KCNJ2) were present in the three probands in this study.

Electrophysiological Studies

For the mutant channel, we screened 50 cells transfected with expression plasmid pIRES-EGFP-I313K that satisfied the Giga-seal resistance requirement. These cells were divided into three groups according to the type of transfection:

Group A: 20 cells transfected with I313K-KCNQ1/KCNE1, 1.0 μg each.

Group B: 18 cells transfected with I313K-KCNQ1 0.5 μg + WT-KCNQ1 0.5 μg + KCNE1 1.0 μg.

Group C: 12 cells transfected with 1.0 μg I313K-KCNQ1 in the absence of KCNE1.

We analyzed the biophysical properties of each cell from these groups; in particular a current-voltage relationship curve with sigmoid appearance denoted its usability. Seventeen cells that did not match the quality control criteria were excluded, and thus 33 cells were included in the final analysis: 10 cells from Group A, 14 cells from Group B, and 9 cells from Group C. Finally, we compared these groups with respect to peak and tail current densities (Table 2). Groups A and C, which had almost no current, did not differ significantly from each other. In Group B cells, in which a 1:1 mass ratio of WT and mutant plasmids were transfected to mimic the situation occurring in heterozygous cardiac cells, the mutant subunit exerted a moderate dominant negative current suppression as evidenced by a >50% reduction in the

TABLE 2

Comparison of Peak and Tail Currents in COS-7 Cells Transfected with Wild-Type and/or Mutant (I313K) KCNQ1 Expression Plasmids in the Presence or Absence of the KCNE1 Expression Plasmid

Transfected Plasmid DNA	Peak Current Density (pA/pF)	Tail Current Density (pA/pF)
WT-KCNQ1/KCNE1 1.0 μg each (n = 10)	70.3 ± 8.6	18.5 ± 3.2
WT-KCNQ1 0.5 μg /KCNE1 1.0 μg (n = 10)	58.8 ± 6.5	12.9 ± 2.3
WT-KCNQ1 1.0 μg (n = 6)	22.0 ± 2.4	4.2 ± 1.3
Untransfected COS-7 negative controls (n = 8)	0.4 ± 0.1	0.2 ± 0.1
I313K-KCNQ1/KCNE1 1.0 μg each (n = 10) (group A)	0.4 ± 0.2* §	0.1 ± 0.1*·§
WT-KCNQ1 0.5 μg/I313K-KCNQ1 0.5 μg /KCNE1 1.0 μg (n = 14) (group B)	14.6 ± 1.6 †	5.0 ± 0.8 †
I313K-KCNQ1 1.0 μg without KCNE1 (n = 9) (group C)	0.5 ± 0.1§	0.1 ± 0.1§

*P < 0.001 versus WT-KCNQ1/KCNE1 1.0 μg each, †P < 0.05 versus WT-KCNQ1 0.5 μg/KCNE1 1.0 μg, §P > 0.5 versus COS-7 untransfected control cells. Data represent the mean ± SEM. I313K= mutant KCNQ1; KCNE1= β subunit of the potassium voltage-gated channel Isk-related family, member 1; KCNQ1= α subunit of the potassium voltage-gated channel KQT-like subfamily, member 1; WT= wild-type.

current density, compared with cells transfected with the same amount of WT plasmid (i.e., WT-KCNQ1 0.5 μg/KCNE1 1.0 μg; Table 2). These findings are depicted in Figure 2. Briefly, cells cotransfected with 1.0 μg of both the WT-KCNQ1 and KCNE1 expression plasmids exhibited a slowly activating outward current compatible with IKs from native cardiac myocytes (Fig. 2A), whereas cotransfection with 1.0 μg each of the I313K-KCNQ1 (mutant) and the KCNE1 expression plasmids (Group A cells) produced no current (Fig. 2B). Cells cotransfected with 0.5 μg WT-KCNQ1 + 0.5 μg I313K-KCNQ1 expression plasmids in the presence of 1.0 μg KCNE1 (Group B cells; Fig. 2C) showed greatly reduced currents, compared with those of cells transfected with either 1.0 μg (Fig. 2A) or 0.5 μg (Fig. 2D) WT-KCNQ1 in the presence of 1.0 μg of KCNE1.

The density-voltage relationship of the peak current during depolarization and the tail current upon repolarization to −40 mV are shown in Table 2 and Figure 3. The shape of the membrane potential versus current density curve was similar among cells transfected with 1.0 μg of WT-KCNQ1,

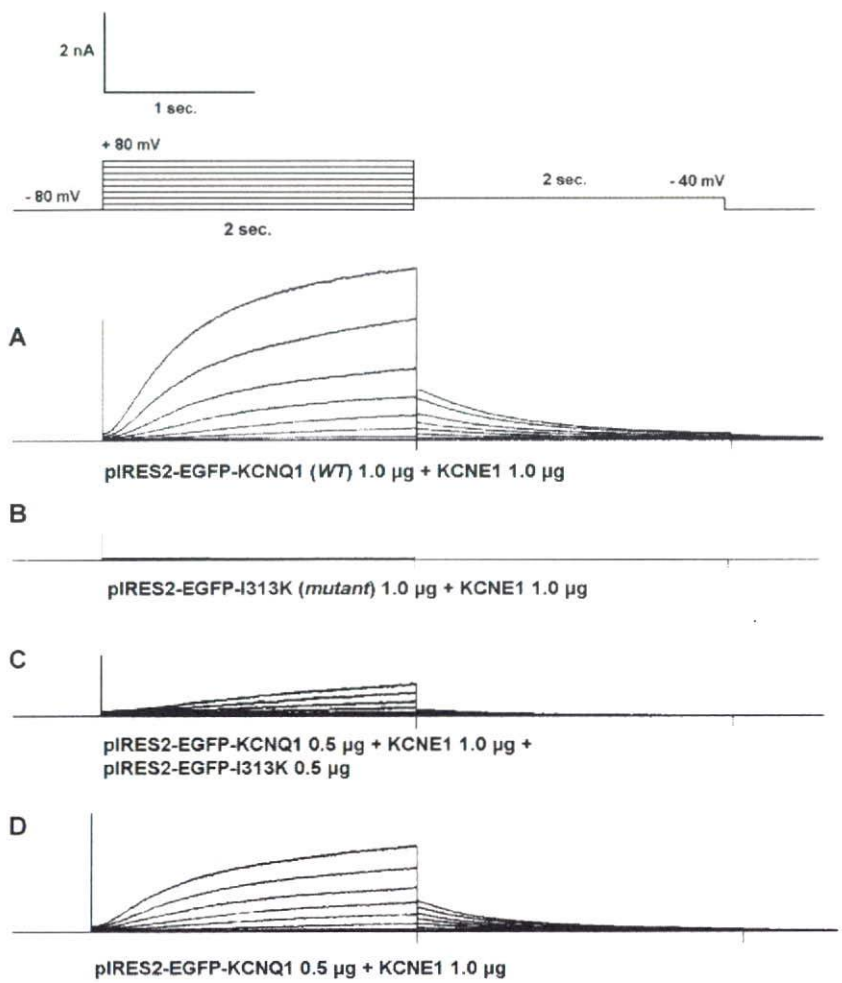

Figure 2. *Whole-cell currents from whole-cell patch-clamp experiments performed on COS-7 cells transfected with pIRES2-EGFP-KCNQ1 (WT) and/or pIRES2-EGFP-I313K (mutant) expression plasmids. Cells were transfected with the following expression plasmids: A: 1.0 µg pIRES2-EGFP-KCNQ1 + 1.0 µg KCNE1, B: 1.0 µg pIRES2-EGFP-I313K + 1.0 µg KCNE1, C: 0.5 µg pIRES2-EGFP-KCNQ1 + 0.5 µg pIRES2-EGFP-I313K + 1.0 µg KCNE1, and D: 0.5 µg pIRES2-EGFP-KCNQ1 + 1.0 µg KCNE1. Pulse protocol and graph scale are shown at the top.*

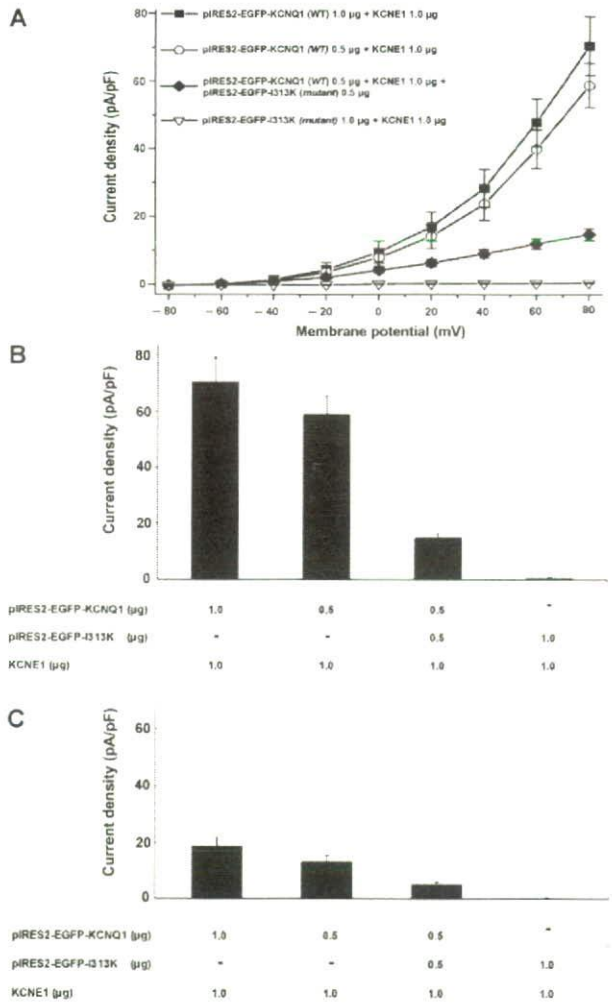

Figure 3. *Current-voltage relationship and current densities from whole-cell patch-clamp experiments performed on COS-7 cells transfected with pIRES2-EGFP-KCNQ1 (WT) and/or pIRES2-EGFP-I313K (mutant) expression plasmids. A: Current-voltage relationship from cells transfected with the following expression plasmids: 1.0 µg pIRES2-EGFP-KCNQ1 (n = 10, closed squares), 0.5 µg pIRES2-EGFP-KCNQ1 (n = 10, open circles), 1.0 µg pIRES2-EGFP-I313K (n = 10, open triangles), or 0.5 µg pIRES2-EGFP-KCNQ1 + 0.5 µg pIRES2-EGFP-I313K (n = 14, closed diamonds). All cells were cotransfected with 1.0 µg of KCNE1 expression plasmid. B: Bar graphs representing the densities of the peak currents (+80 mV) obtained from cells transfected with the indicated amounts of pIRES2-EGFP-KCNQ1 (WT) or pIRES2-EGFP-I313K (mutant) expression plasmids, with an equivalent amount of KCNE1. C: Bar graphs representing the densities of the tail currents obtained upon repolarization to –40 mV from the +80 mV test potential of cells transfected with the indicated amounts of pIRES2-EGFP-KCNQ1 (WT) or pIRES2-EGFP-I313K (mutant) expression plasmids, with equivalent amount of KCNE1.*

0.5 µg of WT-KCNQ1, and 0.5 µg of WT-KCNQ1 + 0.5 µg of I313K-KCNQ1 expression plasmids (in the presence of 1.0 µg KCNE1 expression plasmid for all these situations), but the current densities were different (Fig. 3A). The densities of the peak and tail currents from cells transfected with 0.5 µg WT-KCNQ1 expression plasmid were smaller than those transfected with 1.0 µg of WT-KCNQ1 expression plasmid at all test voltages (in the presence of 1.0 µg KCNE1 expression plasmid). The current densities of cells cotransfected with 0.5 µg WT-KCNQ1 + 0.5 µg I313K-KCNQ1 expression plasmids (i.e., Group B cells) were significantly smaller than those transfected with 0.5 µg WT-KCNQ1 expression plasmid (in the presence of 1.0 µg KCNE1 expression plasmid); however, current densities were nearly undetectable in the Group A cells transfected with 1.0 µg I313K-KCNQ1 expression plasmid (Figs. 2B and 3A-C). The voltage dependency of activation was determined from the tail currents as a function of the test potential. We examined whether cotransfection of WT-KCNQ1 and I313K-KCNQ1 (mutant) expression plasmids altered the activation gating of KCNQ1. The activation curves were fitted to the Boltzmann formula[6]: $I = I_{max}/(1+\exp[(V_{1/2}-V)/k])$, where I is current amplitude, I_{max} is maximal tail current, V is the test pulse potential, $V_{1/2}$ is the half-maximal activation potential, and k is the slope of the activation curve. $V_{1/2}$ and k were 23.2 ± 1.3 mV and 16.7 ± 1.1 mV, respectively, for cells transfected with WT-KCNQ1 0.5 µg + KCNE1 1.0 µg expression plasmids (n = 10 cells), and 23.9 ± 1.8 mV and 17.1±1.6 mV, respectively, for cells transfected with 0.5 µg WT-KCNQ1 + 0.5 µg I313K-KCNQ1 (mutant) + 1.0 µg KCNE1 expression plasmids (Group B; n = 14 cells). Comparison of the respective values for both $V_{1/2}$ and k between the WT and mutant cells revealed no statistically significant differences.

To prove that the mutant KCNQ1 channel lacks potassium current and is responsible for the observed potassium channel defects, we removed the possible influence of KCNE1 by measuring the outward current density of COS-7 cells transfected with 1.0 µg of either the WT-KCNQ1 (Fig. 4A) or I313K-KCNQ1 (mutant) expression plasmid (Group C cells, Fig. 4B) in the absence of the KCNE1 expression plasmid. We also measured the outward current density of untransfected COS-7 cells (Fig. 4C), which have been previously demonstrated to be an effective negative control.[22] Eight untransfected cells reached the Giga-seal resistance requirement and were included in the analysis. The peak and tail currents of cells transfected with 1.0 µg I313K-KCNQ1 (mutant) expression plasmid (Groups A and C) were similar and barely detectable (Fig. 4D; lowest panel) and were similar to the currents measured in untransfected negative control cells, indicating that mutant I313K channels were devoid of K^+ current (Table 2).

Localization of WT- and I313K-KCNQ1 (Mutant) Channels in COS-7 Cells

YFP-tagged pEGFP-N1-KCNQ1 channels were correctly distributed on the plasma membrane, as were CFP-tagged pEGFP-N1-I313K channels (Fig. 2, supplementary online), indicating that the potassium channel defects caused by the I313K mutation were not due to defective trafficking of the mutant protein . Three-dimensional modeling of the KCNQ1 structure suggested that the I313K mutation is positioned at the center of the channel pore (Fig. 3, supplementary online).

Discussion

Analysis of the I313K-KCNQ1 Mutation

In this study, three probands were found to have the same amino acid substitution at residue 313 of KCNQ1, resulting from a double-point mutation at nucleotide positions 938 (T-to-A) and 939 (C-to-A) in the gene, as determined by sequence analysis of all exons. The clinical characteristics of patients who had a different mutation at amino acid

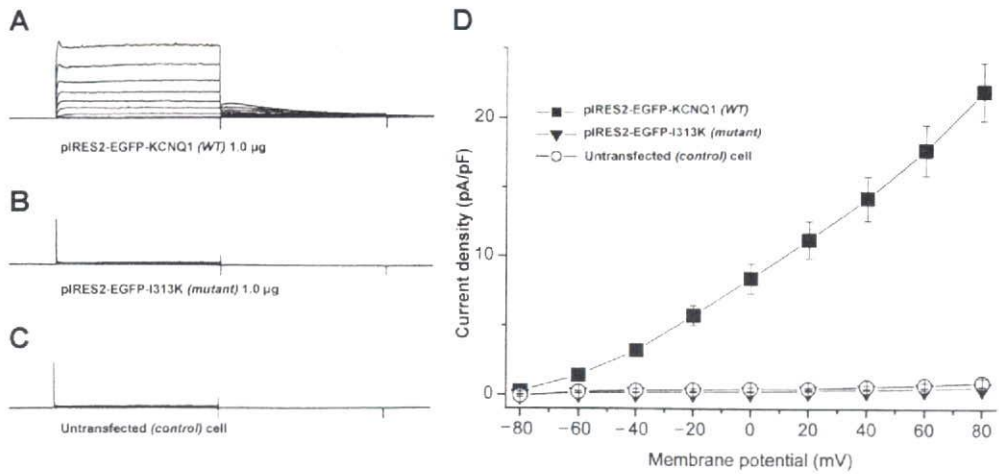

Figure 4. *Current traces and current-voltage relationships from whole-cell patch-clamp experiments performed on COS-7 cells transfected with pIRES2-EGFP-KCNQ1 (WT) or pIRES2-EGFP-I313K (mutant) expression plasmids in the absence of the KCNE1 expression plasmid. A: Current trace obtained from COS-7 cells transfected with 1.0 μg pIRES2-EGFP-KCNQ1 (n = 6). B: Current trace obtained from cells transfected with 1.0 μg pIRES2-EGFP-I313K (n = 9). C: Current trace obtained from untransfected negative control COS-7 cells (n = 8). D: Current-voltage relationship of cells transfected with the following expression plasmids: 1.0 μg pIRES2-EGFP-KCNQ1 (closed squares), 1.0 μg pIRES2-EGFP-I313K (closed triangles), and untransfected control COS-7 cells (open circles).*

residue 313 (I313M single-point mutation: 939 C-to-G) than the probands presented in this study have been described earlier[23,24] where a prolonged QT interval was found, but syncopal attacks were not reported. However, the relationship between I313M mutation and clinical symptoms was not clarified in that study, and the possibility of very rare polymorphisms was not completely excluded. The electrophysiological experiments presented herein showed that I313K mutation results in loss of channel function leading to dominant negative suppression. Consequently, the I313K mutations must be related to the prolongation of QT interval and syncope found in our patients. Also, the possibility of rare polymorphisms was excluded by screening via the direct sequencing method.

In our study, all three probands having an I313K mutation in KCNQ1 had been diagnosed with the dominantly inherited Romano-Ward long QT syndrome (RWS), suggesting that this mutation is responsible for manifestation of the syndrome. This syndrome is associated with characteristic cardiac abnormalities, such as a prolonged QTc interval and T-wave alterations caused by abnormal ventricular repolarization, in addition to clinical presentation of syncopal attacks without congenital deafness.[25]

We report that exogenously expressed I313K-KCNQ1 is sufficient for disruption of K^+ channel function, even when coexpressed with the WT form of the protein, suggesting that I313K-KCNQ1 is a dominant negative mutant. The mutation was not associated with a trafficking defect, and the mutant channel protein was confirmed to appropriately localize at the cell membrane.[5,10,11] Numerous mutations in KCNQ1 have been shown to cause trafficking defects, leading to haploinsufficiency[11] or to a dominant negative effect.[10] These previously identified variations have primarily been the result of missense mutations in the N terminus, the S1–S6 transmembrane domains, the pore region, or the C terminus. The N- and C-terminal domains have been shown to contain a specific sequence linked to endoplasmic reticulum retention, a characteristic that is critical for trafficking of the protein and subsequently for channel surface expression.[26,27] However, mutations identified outside these domains have also been shown to result in trafficking problems of varying intensities.[28] In the present study, we determined that the I313K mutation affects the pore region of the K^+ channel without causing a defect in the trafficking of the protein; this finding is similar to a previously published report describing a KCNQ1 mutant in which residue 275, located in the middle of the S5 segment of KCNQ1, was deleted.[13] Interestingly, the I313K mutation identified in our study is situated at the predicted site of K^+ selectivity in the center of the K^+ channel pore, a structure believed to be critical for K^+ selectivity and conductivity.[29-31]

Mechanism of Functional Loss

K^+ conduction is primarily regulated by the selectivity filter located on the outer region of K^+ channel pores, which is formed by interaction of the P-regions of channel polypeptides with the S6 segment. The S4–S5 linkers also participate in the formation of the selectivity filter.[6,7] The narrow P-region dictates K^+ selectivity, and the amino acid sequence TIGYG within the P-region is now regarded as the K^+ selectivity signature motif.[29,31] Mutations in the pore and the supporting S5 transmembrane regions of the KCNQ1 channel have been thought to disrupt K^+ transport.[6,29,32] In support of this hypothesis, the I313K mutation examined in this study resides within the critical S5 transmembrane region of KCNQ1 and leads to defective K^+ transport, likely due to the substitution of a neutral isoleucine residue with a positively charged lysine. In fact, a previous simulation study showed that charged amino acids within K^+ channels hinder the passage of K^+ ions;[33] therefore, the I313K mutant of KCNQ1 would invariably affect the permeability of K^+ ions through the selectivity filter due to repulsion. Alteration of the pore size and the decreased probability that the channel is open (open probability; P_O) may be involved as additional factors.[34] Taken together, these data suggest that the

I313K mutant of KCNQ1 is responsible for the severe LQTS phenotype common among the probands examined in this study.

Conclusions

An I313K mutation in the selectivity filter of KCNQ1 was confirmed in a family with LQT1 that presented clinically with repetitive syncopal attacks. When exogenously expressed in COS-7 cells, the mutant protein resulted in a loss of K^+ channel function and was shown to act in a dominant-negative manner when coexpressed with WT-KCNQ1, indicating that charge and/or pore size are critical for normal channel function.

Acknowledgments: We thank Dr. Hiroyuki Hanzawa and Dr. Takeshi Takizawa, from the Core Technology Research Laboratories, Sankyo Co. Ltd., Tokyo, Japan, and Dr. Yukio Hosaka from the First Department of Internal Medicine, Niigata University Graduate School of Medical and Dental Sciences, Niigata, Japan for their assistance.

References

1. Chen S, Zhang L, Bryant RM, Vincent GM, Flippin M, Lee JC, Brown E, Zimmerman F, Rozich R, Szafranski P, Oberti C, Sterba R, Marangi D, Tchou PJ, Chung MK, Wang Q: KCNQ1 mutations in patients with a family history of lethal cardiac arrhythmias and sudden death. Clin Genet 2003;63:273-382.
2. Moss AJ, Kass RS: Long QT syndrome: From channels to cardiac arrhythmias. J Clin Invest 2005;115:2018-2024.
3. Marban E: Cardiac channelopathies. Nature 2002;415:213-218.
4. Panaghie G, Tai KK, Abbott GW: Interaction of KCNE subunits with the KCNQ1 K^+ channel pore. J Physiol 2006;1:455-467.
5. Jespersen T, Grunnet M, Olesen SP: The KCNQ1 potassium channel: From gene to physiological function. Physiology (Bethesda) 2005;20:408-416.
6. Seebohm G, Strutz-Seebohm N, Ureche ON, Baltaev R, Lampert A, Kornichuk G, Kamiya K, Wuttke TV, Lerche H, Sanguinetti MC, Lang F: Differential roles of S6 domain hinges in the gating of KCNQ potassium channels. Biophys J 2006;90:2235-2244.
7. Doyle DA, Morais Cabral J, Pfuetzner RA, Kuo A, Gulbis JM, Cohen SL, Chait BT: The structure of the potassium channel: Molecular basis of K+ conduction and selectivity. Science 1998;280: 69-77.
8. Morais-Cabral JH, Zhou Y, MacKinnon R: Energetic optimization of ion conduction rate by the K^+ selectivity filter. Nature 2001;414:37-42.
9. Shimizu W, Horie M, Ohno S, Takenaka K, Yamaguchi M, Shimizu M, Washizuka T, Aizawa Y, Nakamura K, Ohe T, Aiba T, Miyamoto Y, Yoshimasa Y, Towbin JA, Priori SG, Kamakura S: Mutation site-specific differences in arrhythmic risk and sensitivity to sympathetic stimulation in the LQT1 form of congenital long QT syndrome: Multicenter study in Japan. J Am Coll Cardiol 2004;44:117-125.
10. Aizawa Y, Ueda K, Wu LM, Inagaki N, Hayashi T, Takahashi M, Ohta M, Kawano S, Hirano Y, Yasunami M, Aizawa Y, Kimura A, Hiraoka M: Truncated KCNQ1 mutant, A178fs/105, forms hetero-multimer channel with wild-type causing a dominant-negative suppression due to trafficking defect. FEBS Lett 2004;10:145-150.
11. Yamashita F, Horie M, Kubota T, Yoshida H, Yumoto Y, Kobori AT, Kono Y, Haruna T, Tsuji K, Washizuka T, Takano M, Otani H, Sasayama S, Aizawa Y: Characterization and subcellular localization of KCNQ1 with a heterozygous mutation in the C terminus. J Mol Cell Cardiol 2001;33:197-207.
12. Hosaka Y, Hanawa H, Washizuka T, Chinushi M, Yamashita F, Yoshida T, Komura S, Watanabe H, Aizawa Y: Function, subcellular localization and assembly of a novel mutation of KCNJ2 in Andersen's syndrome. J Mol Cell Cardiol 2003;35:409-415.
13. Aizawa Y, Ueda K, Scornik F, Cordiero JM, Wu Y, Desai M, Guerchicoff A, Nagata Y, Iesaka Y, Kimura A, Hiraoka M, Antzelevitch C: A novel mutation in KCNQ1 associated with a potent dominant negative effect as the basis for the LQT1 form of the long QT syndrome. J Cardiovasc Electrophysiol 2007;18:972-977.
14. Saarinen K, Swan H, Kainulainen K, Toivonen L, Viitasalo M, Kontula K: Molecular genetics of the long QT syndrome: Two novel mutations of the KVLQT1 gene and phenotypic expression of the mutant gene in a large kindred. Hum Mutat 1998;11:158-165.
15. Thomas D, Wimmer AB, Karle CA, Licka M, Alter M, Khalil M, Ulmer HE, Kathofer S, Kiehn J, Katus HA, Schoels W, Koenen M, Zehelein J: Dominant-negative I(Ks) suppression by KCNQ1-deltaF339 potassium channels linked to Romano-Ward syndrome. Cardiovasc Res 2005;15:487-497.
16. Kubota T, Shimizu W, Kamakura S, Horie M: Hypokalemia-induced long QT syndrome with an underlying novel missense mutation in S4-S5 linker of KCNQ1. J Cardiovasc Electrophysiol 2000;11:1048-1054.
17. Mohammad-Panah R, Demolombe S, Neyroud N, Guicheney P, Kyndt F, van den Hoff M, Baro I, Escande D: Mutations in a dominant-negative isoform correlate with phenotype in inherited cardiac arrhythmias. Am J Hum Genet 1999;64:1015-1023.
18. Molleman A: *Patch Clamping: An Introductory Guide to Patch Clamp Electrophysiology*. England: John Wiley & Sons, 2003, pp. 107-108.
19. Barhanin J, Lesage F, Guillemare E, Fink M, Lazdunski M, Romey G: K(V)LQT1 and IsK (minK) proteins associate to form the I(Ks) cardiac potassium current. Nature 1996;384:78-80.
20. Sanguinetti MC, Curran ME, Zou A, Shen J, Spector PS, Atkinson DL, Keating MT: Coassembly of K(V)LQT1 and minK (IsK) proteins to form cardiac I(Ks) potassium channel. Nature 1996;384:80-83.
21. Wilson MC, Meredith D, Halestrap AP: Fluorescence resonance energy transfer studies on the interaction between the lactate transporter MCT1 and CD147 provide information on the topology and stoichiometry of the complex in situ. J Biol Chem 2002;277:3666-3672.
22. Demolombe S, Baro I, Pereon Y, Bliek J, Mohammad-Panah R, Pollard H, Morid S, Mannens M, Wilde A, Barhanin J, Charpentier F, Escande D: A dominant negative isoform of the long QT syndrome 1 gene product. J Biol Chem 1998;273:6837-6843.
23. Tanaka T, Nagai R, Tomoike H, Takata S, Yano K, Yabuta K, Haneda N, Nakano O, Shibata A, Sawayama T, Kasai H, Yazaki Y, Nakamura Y: Four novel KVLQT1 and four novel HERG mutations in familial long-QT syndrome. Circulation 1997;95:565-567.
24. Splawski I, Shen J, Timothy KW, Lehmann MH, Priori S, Robinson JL, Moss AJ, Schwartz PJ, Towbin JA, Vincen GM, Keating MT: Spectrum of mutations in long-QT syndrome genes. KVLQT1, HERG, SCN5A, KCNE1, and KCNE2. Circulation 2000;102:1178-1185.
25. Napolitano C, Priori SG, Schwartz PJ, Bloise R, Ronchetti E, Nastoli J, Bottelli G, Cerrone M, Leonardi S: Genetic testing in the long QT syndrome: Development and validation of an efficient approach to genotyping in clinical practice. JAMA 2005;294:2975-2980.
26. Dahimene S, Alcolea S, Naud P, Jourdon P, Escande D, Brasseur R, Thomas A, Baro I, Merot J: The N-terminal juxtamembranous domain of KCNQ1 is critical for channel surface expression: Implications in the Romano-Ward LQT1 syndrome. Circ Res 2006;99:1076-1083.
27. Wilson AJ, Quinn KV, Graves FM, Bitner-Glindzicz M, Tinker A: Abnormal KCNQ1 trafficking influences disease pathogenesis in hereditary long QT syndromes (LQT1). Cardiovasc Res 2005;67:476-486.
28. Kanki H, Kupershmidt S, Yang T, Wells S, Roden DM: A structural requirement for processing the cardiac K+ channel KCNQ1. J Biol Chem 2004;279:33976-33983.
29. Snyders DJ: Structure and function of cardiac potassium channels. Cardiovasc Res 1999;42:377-390.
30. Roden DM: Defective ion channel function in the long QT syndrome: Multiple unexpected mechanisms. J Mol Cell Cardiol 2001;33:185-187.
31. Berneche S, Roux B: A gate in the selectivity filter of potassium channels. Structure 2005;13:591-600.
32. Jiang Y, Lee A, Chen J, Cadene M, Chait BT, MacKinnon R: The open pore conformation of potassium channels. Nature 2002;417:523-526.
33. Allen TW, Bliznyuk A, Rendell AP, Kuyucak S, Chung SH: The potassium channel: Structure, selectivity and diffusion. J Chem Phys 2000;112:8191-8204.
34. Seebohm G, Westenskow P, Lang F, Sanguinetti MC: Mutation of colocalized residues of the pore helix and transmembrane segments S5 and S6 disrupt deactivation and modify inactivation of KCNQ1 K^+ channels. J Physiol 2005;563:359-368.

Supplementary Material

The following supplementary material is available for this article:

Figure S1. Schematic presentation of the various domains of the KCNQ1 potassium channel and the site of mutation (I313K) in the selectivity filter of the channel pore is shown at left. The single transmembrane domain ancillary subunit minK (known as KCNE1), which interacts with KCNQ1 to form the cardiac IKs, is shown at right. The oval-and-balls portion of the drawing represents the cell membrane (online supplementary).
Figure S2. Subcellular localization of WT- and mutant-KCNQ1 ectopically expressed in COS-7 cells. A: Confocal microscopic image of yellow fluorescent protein (YFP)-tagged WT-KCNQ1 channels coexpressed with KCNE1 showing localization to the plasma membrane. B: Confocal microscopic image of cyan fluorescent protein (CFP)-tagged I313K-KCNQ1 (mutant) channels coexpressed with KCNE1 showing localization to the plasma membrane (online supplementary).
Figure S3. Computerized three-dimensional ribbon diagram showing the predicted location of the I313K mutation (red) at the selectivity filter and central pore of the KCNQ1 potassium channel. The model of KCNQ1 was built using Swiss-Model (Glaxo Welcome- http:// www.expasy.org/swissmod/SWISS-MODEL.html; online supplementary).

This material is available as part of the online article from:
http://www.blackwell-synergy.com/doi/abs/10.1111/j.1540-8167.2007.01076.x
(This link will take you to the article abstract).

Please note: Blackwell Publishing is not responsible for the content or functionality of any supplementary materials supplied by the authors. Any queries (other than missing material) should be directed to the corresponding author for the article.

Sodium channel β1 subunit mutations associated with Brugada syndrome and cardiac conduction disease in humans

Hiroshi Watanabe,[1,2] Tamara T. Koopmann,[3] Solena Le Scouarnec,[4,5,6] Tao Yang,[1] Christiana R. Ingram,[1] Jean-Jacques Schott,[4,5,6,7] Sophie Demolombe,[4,5,6] Vincent Probst,[4,5,6,7] Frédéric Anselme,[8] Denis Escande,[4,5,6,7] Ans C.P. Wiesfeld,[9] Arne Pfeufer,[10,11] Stefan Kääb,[12] H.-Erich Wichmann,[11,12] Can Hasdemir,[13] Yoshifusa Aizawa,[2] Arthur A.M. Wilde,[3] Dan M. Roden,[1] and Connie R. Bezzina[3]

[1]Department of Medicine and Pharmacology, Vanderbilt University School of Medicine, Nashville, Tennessee, USA. [2]Division of Cardiology, Niigata University Graduate School of Medical and Dental Sciences, Niigata, Japan. [3]Heart Failure Research Center, Department of Experimental Cardiology, Academic Medical Center, University of Amsterdam, Amsterdam, The Netherlands. [4]INSERM, UMR915, l'institut du thorax, Nantes, France. [5]Université de Nantes, Nantes, France. [6]CNRS ERL3147, Nantes, France. [7]CHU Nantes, l'institut du thorax, Service de Cardiologie, Nantes, France. [8]CHU Rouen, Département de Cardiologie, Rouen, France. [9]Department of Cardiology, Thoraxcenter, University Medical Center Groningen, Groningen, The Netherlands. [10]Institut für Humangenetik, Technical University of Munich, Munich, Germany. [11]Helmholtz Zentrum Munich, German Research Center for Environmental Health, Neuherberg, Germany. [12]Department of Medicine I, Ludwig-Maximilians-University Munich, Klinikum Großhadern, Munich, Germany. [13]Department of Cardiology, Ege University School of Medicine, Izmir, Turkey.

Brugada syndrome is a genetic disease associated with sudden cardiac death that is characterized by ventricular fibrillation and right precordial ST segment elevation on ECG. Loss-of-function mutations in *SCN5A*, which encodes the predominant cardiac sodium channel α subunit $Na_V1.5$, can cause Brugada syndrome and cardiac conduction disease. However, *SCN5A* mutations are not detected in the majority of patients with these syndromes, suggesting that other genes can cause or modify presentation of these disorders. Here, we investigated *SCN1B*, which encodes the function-modifying sodium channel β1 subunit, in 282 probands with Brugada syndrome and in 44 patients with conduction disease, none of whom had *SCN5A* mutations. We identified 3 mutations segregating with arrhythmia in 3 kindreds. Two of these mutations were located in a newly described alternately processed transcript, β1B. Both the canonical and alternately processed transcripts were expressed in the human heart and were expressed to a greater degree in Purkinje fibers than in heart muscle, consistent with the clinical presentation of conduction disease. Sodium current was lower when $Na_V1.5$ was coexpressed with mutant β1 or β1B subunits than when it was coexpressed with WT subunits. These findings implicate *SCN1B* as a disease gene for human arrhythmia susceptibility.

Introduction

Voltage-gated sodium channels are critical for the generation and propagation of the cardiac action potential, and mutations in *SCN5A*, the gene encoding the major pore-forming sodium channel α subunit in the heart ($Na_V1.5$), cause multiple cardiac arrhythmia syndromes (1–4). Mutations producing enhanced inward current during the course of the action potential plateau, often as a consequence of destabilized fast inactivation of the channel, cause long QT syndrome type 3 (LQT3; OMIM 603830) (1). On the other hand, a reduction in sodium current leads to cardiac conduction disease, which may be progressive (OMIM 113900) (2, 3), and Brugada syndrome (OMIM 601144), characterized by ST segment elevation in the right precordial leads (V1 to V3) of the 12-lead ECG and episodes of ventricular fibrillation (4). Multiple mechanisms have been described that reduce sodium current in these syndromes, including altered gating of the channel or reduced cell-surface expression (5). In addition, mutations in *SCN5A* may manifest with an overlap of these different phenotypes (6–10). However, mutations in *SCN5A* are found in fewer than 30% of patients with Brugada syndrome, indicating involvement of other genes (11). A mutation in the glycerol-3-phosphate dehydrogenase 1–like gene (*GPD1L*) has recently been reported in a large kindred with Brugada syndrome (12); however, *GPD1L* mutations are rare in Brugada syndrome (13). Antzelevitch et al. have recently reported mutations in the gene encoding the L-type calcium channel (*CACNA1C*) or its β2b subunit (*CACNB2b*) in Brugada syndrome patients with unusually short QT intervals (14), but the frequency of these defects as a cause for more-typical Brugada syndrome is unknown. *SCN5A* mutations are also not identified in the majority of patients with cardiac conduction disease (15).

Sodium channels are multisubunit protein complexes composed not only of pore-forming α subunits but also of multiple other protein partners including auxiliary function-modifying β subunits (16, 17). In humans, 4 sodium channel β subunits (β1 to β4, encoded by *SCN1B* to *SCN4B*) have been identified, and they share a common predicted protein topology: a large extracellular N-terminal domain (including an immunoglobulin-like domain), a single transmembrane segment, and an intracellular C-terminal domain (16). Functions attributed to β subunits include an increase in sodium channel expression at the cell surface, modulation of channel gating and voltage dependence, and a role in cell adhesion and recruitment of cytosolic proteins such as ankyrin-G (16).

The β1 transcript arises from splicing of exons 1–5 of the *SCN1B* gene (Figure 1, A and B). More recently, a second transcript has been described, arising from splicing of exons 1–3 with retention of a segment of intron 3 (termed exon 3A), leading to an alternate 3′ sequence

Conflict of interest: The authors have declared that no conflict of interest exists.
Citation for this article: *J. Clin. Invest.* **118**:2260–2268 (2008). doi:10.1172/JCI33891.

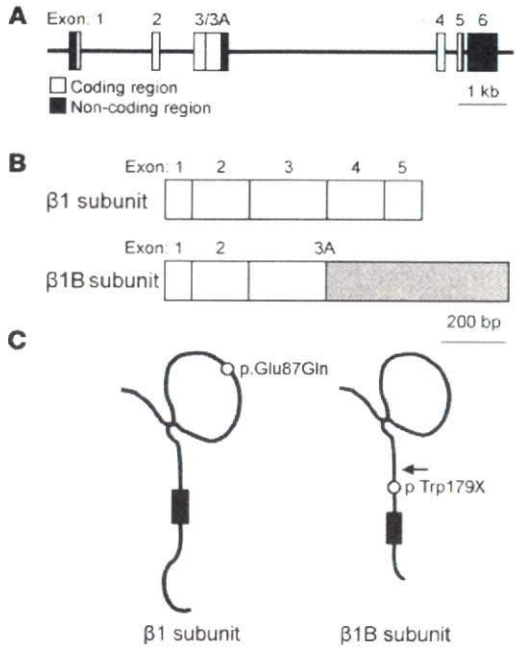

Figure 1
Structure of β1 and β1B subunits. (**A**) Genomic structure of *SCN1B*. (**B**) Extension of exon 3 (c.208–458) into intron 3 creates a novel 3′ end of the transcript (exon 3A, c.208–978) and generates an alternate transcript encoding β1B. The gray region indicates the unique sequence of exon 3A. (**C**) Predicted topology of β1 and β1B. The β1B protein has unique juxtamembrane, transmembrane, and intracellular domains. The arrow indicates the initial amino acid of the β1B-specific segment. Circles indicate the locations of the mutations.

(Figure 1, A and B) (18, 19). This latter transcript encodes the β1B subunit, which, in spite of the different 3′ sequence, has a predicted protein topology similar to that of β1 (Figure 1C) (19). The β1B subunit has been shown to increase a neuronal sodium current ($Na_v1.2$) (19), but its effects on $Na_v1.5$ current have not yet been investigated, although β1 and β1B are both expressed in heart (19, 20).

Since loss-of-function $Na_v1.5$ mutations cause conduction disease and Brugada syndrome, one could envision that mutations in sodium channel β subunits could also underlie these disorders by decreasing sodium current. Therefore, we tested the hypothesis that mutations in *SCN1B* coding sequences, for either β1 or β1B, underlie cases of conduction disease and Brugada syndrome. We identified 3 mutations segregating with arrhythmia in 3 kindreds, and 2 of the mutations were located in the newly described β1B transcript. Both β1 and β1B transcripts were expressed in the human heart and were abundant in Purkinje fibers that play a critical role in electric pulse conduction in heart. Electrophysiologic study of heterologously expressed sodium channels revealed loss of sodium current with mutant subunits.

Results

Mutation analysis and clinical data. We screened 282 probands with Brugada syndrome and 44 with conduction disease for mutations in exons 1–5 of *SCN1B* encoding the β1 subunit and in exon 3A retained in the β1B transcript (Figure 1, A and B). *SCN5A* coding region mutations had been previously excluded in all 326 subjects. Three variants were identified in probands and family members (Figure 2A). These variants were absent in 1,404 population controls (see Methods).

A missense mutation, c.259G→C (Figure 2B) in exon 3, resulting in p.Glu87Gln within the extracellular immunoglobulin loop of the protein (Figure 1C) was identified in a Turkish kindred affected by conduction disease (family 1; Figure 2A). Alignment of the β1 subunit amino acid sequence from multiple species demonstrated that Glu87 is highly conserved, supporting the importance of glutamate at this position (Figure 2C). The proband was a 50-year-old white Turkish female (II-1) who presented with palpitations and dizziness. Physical examination and echocardiography were normal, and her ECG showed complete left bundle branch block. A clinical electrophysiological study revealed a prolonged His-ventricle interval of 80 ms and inducible atrioventricular nodal reentrant tachycardia; complete atrioventricular block occurred following atrial programmed stimulation and during induced tachycardia. A dual-chamber pacemaker was implanted with resolution of symptoms. The same mutation was found in her brother (II-3), who had bifascicular block (right bundle branch block and left anterior hemiblock), and her mother (I-2), who had a normal ECG. There was no family history of syncope, sudden cardiac death, or epilepsy.

A nonsense mutation, c.536G→A in exon 3A (Figure 1B and Figure 2D), was identified in a French kindred affected with Brugada syndrome and conduction disease (family 2; Figure 2A). This mutation results in p.Trp179X and is predicted to generate a prematurely truncated protein lacking the membrane-spanning segment and intracellular portion of the protein (Figure 1C). The proband was a 53-year-old white male (II-4) who presented with chest pain. Physical examination, echocardiography, and coronary angiography were normal. His ECG showed ST segment elevation typical of Brugada syndrome and conduction abnormalities (prolonged PR interval of 220 ms and left anterior hemiblock; Figure 2E) (21). Ventricular fibrillation was induced by programmed electrical stimulation in basal state (in the absence of drugs). The same mutation was detected in his brother (II-1), nephew (III-1), and sister (II-2). The brother had no palpitations or history of syncope. His baseline ECG showed left anterior hemiblock and minor ST segment elevation suggestive of Brugada syndrome at baseline (type II saddleback abnormality; ref. 21); with flecainide challenge, the ST segment elevation was further exaggerated but did not meet criteria for a diagnostic (type I) pattern. The nephew had right bundle branch block and type II Brugada syndrome ECG after flecainide challenge, and the sister had a normal ECG and a negative flecainide test. There was no family history of tachyarrhythmias, syncope, sudden cardiac death, or epilepsy.

A different nonsense mutation, c.537G→A in exon 3A (Figure 2D), resulting in p.Trp179X, affecting the same codon as in family 2, was identified in a Dutch kindred (family 3; Figure 2A). The proband was a 17-year-old white female (II-1). Physical examination and echocardiography were normal, and a flecainide test for Brugada syndrome was negative. Her ECG showed right bundle branch block and prolonged PR interval of 196 ms (normal upper limit in teenagers, 180 ms) (22). The same mutation was found in her father (I-1), with normal ECG and negative flecainide test. The family history was negative for syncope, sudden cardiac death, or epilepsy.

β1 and β1B transcript expression. To confirm and extend previous reports that β1B is expressed in brain, heart, skeletal muscle, and other organs (19), we used quantitative real-time PCR in nondiseased

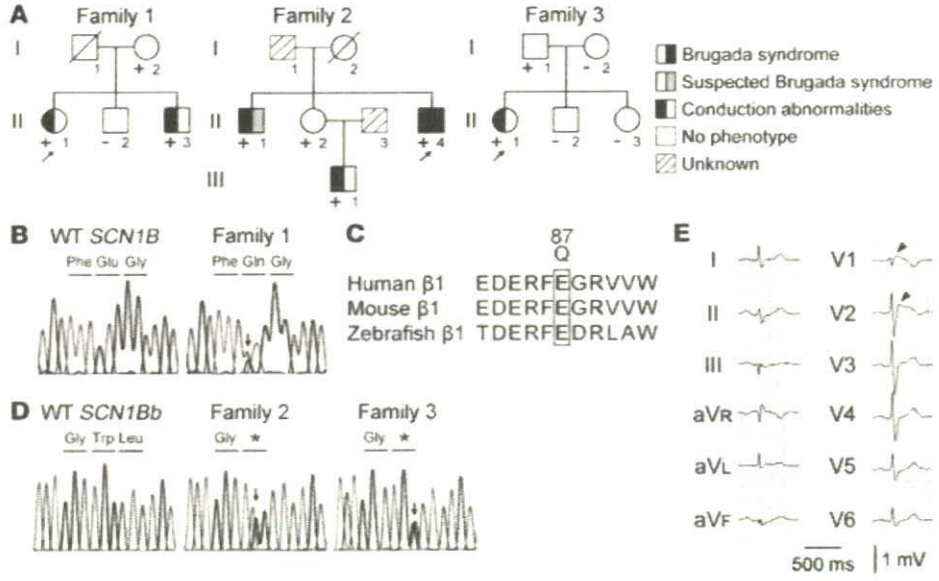

Figure 2

SCN1B mutations found in patients with Brugada syndrome and conduction disease. (**A**) Pedigrees and phenotypes of the families affected by Brugada syndrome and/or conduction disease. Individuals carrying the mutation are indicated (+). Individuals who tested negative for the mutation are indicated (–). Individuals I-1 from family 1; and I-1, I-2, and II-3 from family 2 did not undergo genetic testing. Arrows indicate probands. (**B**) The c.259G→C mutation in *SCN1B* resulting in p.Glu87Gln found in family 1. (**C**) Alignment of β1 across species showing the high conservation of Glu87. (**D**) The c.536G→A (middle) and c.537G→A (right) mutations in exon 3A of β1B, both resulting in p.Trp179X found in families 2 and 3, respectively. (**E**) Twelve-lead ECG from the proband of family 2 (II-4). The arrowheads indicate ST-segment elevation typical of Brugada syndrome.

human heart. Both β1 and β1B transcripts were detected in right and left ventricles and in Purkinje fibers (Figure 3). The β1 transcript level was higher in Purkinje fibers (which make up the conduction system in the ventricle) than left- (2.4-fold; $P < 0.05$) and right-ventricular (1.6-fold; P = NS) free walls. β1B transcript levels showed an even greater difference: Purkinje fibers versus left- (4.8-fold; $P < 0.001$) and right-ventricular (3.7-fold; $P < 0.001$) free walls. Levels of both transcripts were also slightly (but not statistically significantly) higher in right- versus left-ventricular free wall (1.5-fold and 1.3-fold for β1 and β1B transcripts, respectively).

Cellular electrophysiology. The effects of mutant and WT β1 and β1B variants on $Na_V1.5$ sodium current were assessed using the whole-cell patch-clamp technique in transfected CHO cells. As described in Methods, bicistronic expression vectors encoding a reporter (GFP or DsRed) with or without β subunits were cotransfected with expression vector encoding $Na_V1.5$. Currents were compared in cells transfected with *SCN5A* alone or *SCN5A* plus WT, mutant, or both β subunits.

Figure 4A shows representative current traces in cells expressing $Na_V1.5$ alone and $Na_V1.5$ plus WT or mutant β1B (p.Trp179X β1B) or their combination; current densities at –30 mV are summarized in Figure 4B. Coexpression of $Na_V1.5$ with WT β1B significantly increased sodium current density over $Na_V1.5$ alone, by 69%, while currents recorded with p.Trp179X β1B coexpression were no different from $Na_V1.5$ alone. Similarly, while coexpression of WT subunit with $Na_V1.5$ shifted the voltage dependence of both activation and inactivation to more negative potentials compared with those with $Na_V1.5$ alone, no such shift was observed with the mutant (Figure 4C and Table 1). This result indicates that while WT β1B modulates $Na_V1.5$ gating (in a fashion similar to WT β1; see below), the mutant exerts no such effect. Coexpression of WT or mutant β1B with $Na_V1.5$ did not alter recovery from inactivation (Figure 4D and Table 1).

To examine whether expression of the mutant influences the effect of WT β1B on $Na_V1.5$ current (e.g., to produce a dominant negative action), cells were transfected with $Na_V1.5$ and varying amounts of WT and p.Trp179X β1B. Figure 4B shows that the sodium current increase over $Na_V1.5$ alone recorded with transfection of 1 μg of both β1B subunit constructs was identical to the increase with that of 1 μg of WT β1B. In addition, the increase in sodium current recorded with transfection of 0.5 μg of both β1B subunit constructs was 51% of that with 1 μg of β1B alone. These data indicate that p.Trp179X β1B does not exert a dominant negative effect on WT β1B function and further support the finding that the mutant, unlike WT, does not affect sodium channel function.

Figure 5A shows representative current traces of $Na_V1.5$ and $Na_V1.5$ coexpressed with WT and/or mutant β1 (p.Glu87Gln β1); current densities are summarized in Figure 5B. Coexpression of $Na_V1.5$ with WT β1 significantly increased sodium current density at –30 mV, by 76%, while coexpression with mutant β1 (p.Glu87Gln β1) did not increase the sodium current. The increase in sodium current recorded with coexpression of $Na_V1.5$ and 1 μg of both WT and p.Glu87Gln β1 (+20%) was markedly smaller than the increase with coexpression of $Na_V1.5$ with 1 μg WT β1 alone (+76%), indicating that this mutant exerts a dominant negative effect on WT β1 function. Figure 5C shows that WT β1 produced negative shifts in the voltage dependence of $Na_V1.5$ activation and inactivation similar to those observed with WT β1B. p.Glu87Gln β1 shifted the voltage dependence of inactivation to negative potentials (similar to WT β1) but did not alter the voltage dependence of activation (Table 2). Coexpression of WT or mutant β1 with $Na_V1.5$ did not alter recovery from inactivation (Figure 5D and Table 2).

Since Glu87 is located in a region of the protein common to both β1 and β1B, we also studied the effects of p.Glu87Gln β1B on $Na_V1.5$ current properties (Supplemental Figure 1 and Supplemental Table 1; supplemental material available online with this article; doi:10.1172/JCI33891DS1). While WT β1B increased $Na_V1.5$ current by 69% (Figure 4), p.Glu87Gln β1B did not increase the sodium current compared with $Na_V1.5$ alone. Similarly, WT β1B produced a negative shift in voltage dependence of both activation and inactivation (Table 1), while p.Glu87Gln β1B shifted only the voltage dependence of inactivation compared with $Na_V1.5$ alone. As with the other β subunit

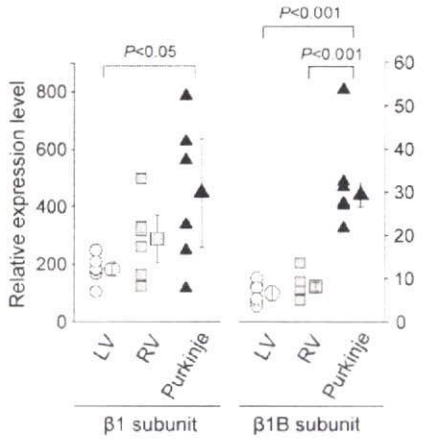

Figure 3
Expression profile of β1 and β1B transcripts in nondiseased human ventricular tissue as determined by quantitative real-time PCR. Relative expression levels of the β1 and β1B subunits are presented, normalized to those of *HPRT1* in LV (circles), RV (squares), and Purkinje fibers (triangles). Tissues for each group were collected from 6 human donors (nondiseased hearts, $n = 6$). Data points indicate the average of 2 measurements in each tissue sample. Larger symbols and error bars indicate median ± median absolute deviation for all samples.

constructs studied, there was no change in recovery from inactivation. Thus, the effects of p.Glu87Gln were comparable in the β1 and the β1B backbones.

Since Glu87 is located in a region of the protein common to both β1 and β1B, we also studied the effects of p.Glu87Gln β1B on $Na_V1.5$ current properties (Supplemental Figure 1 and Supplemental Table 1). While WT β1B increased $Na_V1.5$ current by 69% (Figure 4), p.Glu87Gln β1B did not increase the sodium current compared with $Na_V1.5$ alone. Similarly, WT β1B produced a negative shift in voltage dependence of both activation and inactivation (Table 1), while p.Glu87Gln β1B shifted only the voltage dependence of inactivation compared with $Na_V1.5$ alone. As with the other β subunit constructs studied, there was no change in recovery from inactivation. Thus, the effects of p.Glu87Gln were comparable in the β1 and the β1B backbones.

Discussion

In this study, we provide what we believe to be the first report of mutations in *SCN1B* sequences encoding the β1 and β1B transcript variants in patients with conduction disease and/or Brugada syndrome. Further, we provide new data indicating that β1 and β1B transcripts in the heart vary by region; greater expression in Purkinje fibers is consistent with the conduction system phenotype we describe in mutation carrier patients. Finally, we demonstrate that the β1 and β1B variants modulate function of the major cardiac sodium channel α subunit $Na_V1.5$ and that the identified *SCN1B* mutations blunt or inhibit this effect.

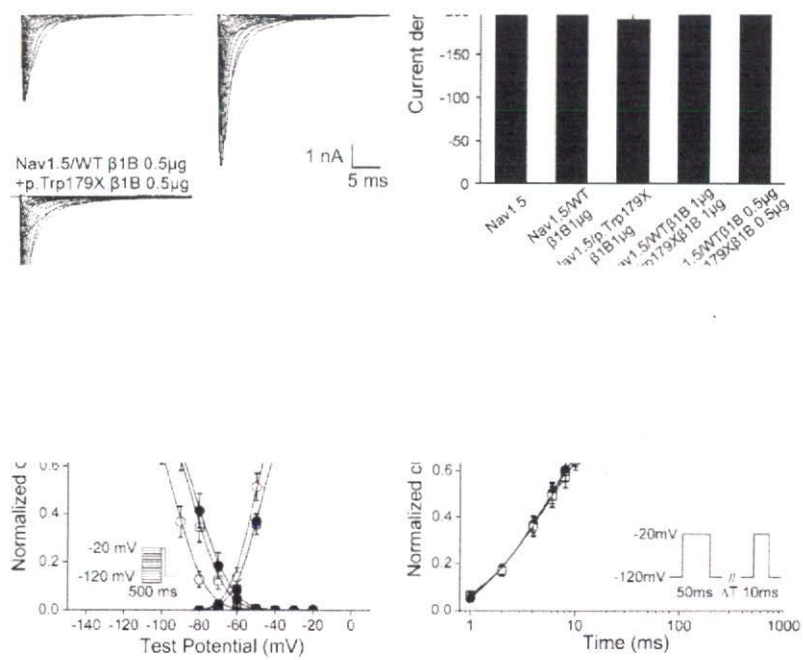

Figure 4
Electrophysiological characteristics of the p.Trp179X β1B mutant. (**A**) Representative traces of sodium current demonstrating an increase in sodium current with WT but not mutant subunit. (**B**) Sodium current density at –30 mV for $Na_V1.5$ alone ($n = 29$), $Na_V1.5$ coexpressed with WT β1B ($n = 28$), $Na_V1.5$ coexpressed with p.Trp179X β1B ($n = 18$), $Na_V1.5$ coexpressed with WT β1B plus p.Trp179X β1B (1 μg for each; $n = 14$), and $Na_V1.5$ coexpressed with WT β1B plus p.Trp179X β1B (0.5 μg for each; $n = 10$). (**C**) Voltage dependence of activation and inactivation. Filled circles, open circles, and squares indicate $Na_V1.5$ alone, $Na_V1.5$ coexpressed with WT β1B, and $Na_V1.5$ coexpressed with p.Trp179X β1B, respectively. The pulse protocol used to study the voltage dependence of inactivation is shown in the inset. (**D**) Recovery from inactivation. Biophysical properties are provided in Table 1.

Table 1
Biophysical parameters of WT and mutant β1B

	Voltage dependence of activation			Voltage dependence of inactivation			Recovery from inactivation		
	$V_{1/2}$, mV	k, mV	n	$V_{1/2}$, mV	k, mV	n	τ_f, ms (amplitude, %)[A]	τ_s, ms (amplitude, %)[A]	n
$Na_V1.5$	−46.2 ± 1.0	7.1 ± 0.4	29	−83.8 ± 1.8	7.6 ± 0.2	17	7.7 ± 1.1 (87.2 ± 1.1)	56.4 ± 9.8 (11.6 ± 1.0)	12
$Na_V1.5$/WT β1B	−50.6 ± 0.7[B]	6.3 ± 0.3	28	−94.2 ± 1.3[A]	7.6 ± 0.2	14	7.4 ± 1.0 (86.5 ± 1.2)	43.3 ± 8.6 (13.1 ± 1.1)	14
$Na_V1.5$/p.Trp179X β1B	−46.3 ± 1.3[C]	6.5 ± 0.4	18	−85.2 ± 2.0[B]	6.6 ± 0.3	15	8.2 ± 1.0 (91.8 ± 1.1)	58.0 ± 11.9 (7.8 ± 1.0)	12

Values are shown as mean ± SEM. [A]The percentages refer to the properties of the overall time constants contributed by the 2 components τ_f and τ_s. [B]$P < 0.01$ versus $Na_V1.5$ alone. [C]$P < 0.01$ versus $Na_V1.5$/WT β1B.

The 3 mutations were identified in 3 probands with conduction disease and/or Brugada syndrome as well as in other family members with or without these arrhythmia phenotypes. Formal linkage analysis was not possible because the families are too small and penetrance is incomplete. Thus, evidence in support of disease causality of these mutations (beyond their identification in subjects with clinical phenotypes) includes the findings that both β1 and β1B transcripts are expressed in heart and that the mutant subunits (p.Glu87Gln β1, p.Glu87Gln β1B, and p.Trp179X β1B) did not increase $Na_V1.5$ currents in heterologous expression experiments, while WT β1 and β1B did. Incomplete penetrance, a well-recognized feature of the monogenic arrhythmia syndromes (12, 23), was observed. For *SCN5A* mutations linked to Brugada syndrome, penetrance as low as 12.5% has been described (24). A role for sex, age, and genetic modifiers (e.g., common polymorphisms) is suspected (5, 25, 26), but the mechanisms for this common clinical finding remain poorly understood.

Two types of mutations were identified. The c.536G→A and c.537G→A mutations in exon 3A both result in a stop codon at position 179, predicted to generate a β1B protein lacking the transmembrane and cytoplasmic domains and thus unable to integrate into the sarcolemma and to associate with $Na_V1.5$. Thus, the a priori assumption is that a mutation such as this will cause disease by simple haploinsufficiency. The electrophysiologic data support this idea, since coexpression of p.Trp179X β1B failed to increase $Na_V1.5$ current and did not modulate the effect of the WT β1B protein. Furthermore, the voltage dependencies of activation and inactivation of $Na_V1.5$ coexpressed with p.Trp179X β1B were the same as those for $Na_V1.5$ alone, in contrast to the shifts observed with WT β1B. While *Scn1b*-knockout mice display clear ECG changes (27), studies with young (17- to 18-day-old) heterozygotes identified no difference from WT. Since age-related changes in conduction are a recognized feature of cardiac conduction disease and conduction delay is one of the proposed mechanisms of Brugada syndrome (2, 28), aging may be important for the β subunit–mediated phenotype.

On the other hand, the c.259G→C mutation leads to an amino acid substitution (p.Glu87Gln) within the extracellular domain of the

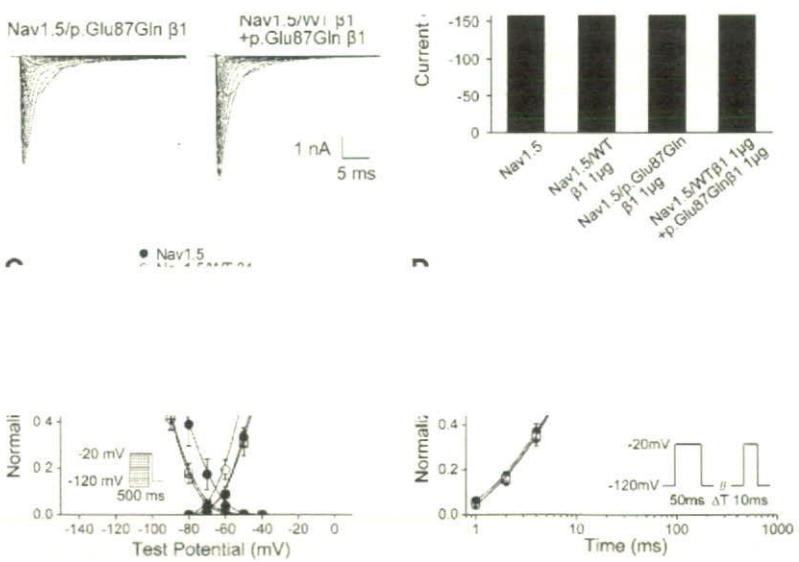

Figure 5
Electrophysiological characteristics of the p.Glu87Gln mutant. (**A**) Representative traces of sodium current. (**B**) Current density at −30 mV for $Na_V1.5$ alone (n = 13), $Na_V1.5$ coexpressed with WT β1 (n = 17), $Na_V1.5$ coexpressed with p.Glu87Gln β1 (n = 18), and $Na_V1.5$ coexpressed with WT β1 plus p.Glu87Gln β1 (n = 15). (**C**) Voltage dependence of activation and inactivation. Filled circles, open circles, and squares indicate $Na_V1.5$ alone, $Na_V1.5$ coexpressed with WT β1, and $Na_V1.5$ coexpressed with p.Glu87Gln β1, respectively. (**D**) Recovery from inactivation. Biophysical properties are provided in Table 2.

Table 2
Biophysical parameters of WT and mutant β1

	Voltage dependence of activation			Voltage dependence of inactivation			Recovery from inactivation		
	$V_{1/2}$, mV	k, mV	n	$V_{1/2}$, mV	k, mV	n	τ_f, ms (amplitude, %)[A]	τ_s, ms (amplitude, %)[A]	n
$Na_V1.5$	−46.1 ± 1.7	7.8 ± 0.4	13	−85.1 ± 3.2	7.3 ± 0.5	12	8.2 ± 1.2 (88.2 ± 1.3)	52.4 ± 7.9 (11.0 ± 1.3)	9
$Na_V1.5$/WT β1	−50.6 ± 1.4[B]	7.3 ± 0.4	17	−92.6 ± 1.4[A]	6.4 ± 0.2	12	7.5 ± 1.1 (84.2 ± 1.3)	43.1 ± 4.6 (14.1 ± 1.3)	13
$Na_V1.5$/p.Glu87Gln β1	−44.9 ± 1.4[C]	7.7 ± 0.4	18	−92.5 ± 1.7[A]	6.8 ± 0.2	12	7.7 ± 1.1 (89.1 ± 1.1)	52.0 ± 9.5 (10.4 ± 1.1)	10

Values are shown as mean ± SEM. [A]The percentages refer to the properties of the overall time constants contributed by the 2 components τ_f and τ_s. [B]$P < 0.05$ versus $Na_V1.5$ alone. [C]$P < 0.05$ versus $Na_V1.5$ /WT β1.

protein. The electrophysiological data demonstrate that the mutant subunit did modulate $Na_V1.5$ gating (shift in the voltage dependence of inactivation, in either the β1 or β1B background), supporting the idea that it associates with $Na_V1.5$ at the cell surface. In addition, in contrast to the p.Trp179X β1B, p.Glu87Gln did exert a dominant negative effect on the WT subunit. Thus, the 3 mutations lead to a decrease in $Na_V1.5$ current through somewhat different mechanisms. This reduction of current is consistent with the conduction disease and Brugada syndrome phenotypes of the patients.

Normal impulse propagation in the atria, ventricles, and Purkinje network is critically dependent on normal sodium channel function. Dysfunction of the sodium channel leads to conduction delay, and loss-of-function mutations in *SCN5A* have been described in isolated conduction disease unassociated with structural heart disease (2, 3). Thus, our finding of *SCN1B* mutations associated with reduced sodium current in patients with conduction disease is consistent with previous studies of the mechanism of this disorder. The preferential expression of the β1 and β1B transcripts in human Purkinje fibers further supports the prominent conduction delay seen as part of the clinical phenotypes.

Loss-of-function mutations in *SCN5A* were the first reported cause of the Brugada syndrome (4). These mutations reduce sodium current by reducing $Na_V1.5$ cell surface expression and/or altering gating (4, 5, 29). A common view is that in epicardial cells, this reduction in sodium current produces marked action potential shortening, attributed to an "unopposed" early transient outward potassium current. By contrast, reduction of sodium current in endocardial cells is thought to produce only modest action potential shortening. The resultant increased heterogeneity of repolarization predisposes to rapid reentry, resulting in ventricular fibrillation (4, 30). A common feature in Brugada syndrome — consistent with reduced sodium current — is slowed conduction (28, 31). Indeed, an alternate proposed mechanism suggests that the characteristic right-precordial ST-segment elevation on the ECG and initiation of arrhythmias is attributable primarily to right-ventricular outflow tract conduction delay (28). The trend to higher expression levels of β1B in right ventricle may thus contribute to the Brugada syndrome phenotype.

This idea is further supported by functional studies in a single large kindred in which a *GPD1L* mutation was linked to Brugada syndrome: coexpression of mutant *GPD1L* with $Na_V1.5$ was reported to decrease sodium current, consistent with the observation that loss-of-function mutations in *SCN5A* cause Brugada syndrome (12). In principle, reduction in L-type calcium current might also produce differential effects in epicardial and endocardial sites and thus cause Brugada syndrome; rare kindreds with this mechanism have now been described (14).

Conduction disease was observed in families 1 and 3, while in family 2, mutation carriers presented either solely with conduction disease or conduction disease in combination with ECGs typical of Brugada syndrome. This phenomenon of overlapping clinical phenotypes is common in individuals with *SCN5A* mutations leading to loss of sodium channel function (6, 7), and conversely, in vitro electrophysiologic analysis of *SCN5A* mutations linked to Brugada syndrome or isolated conduction disease consistently reveals loss of $Na_V1.5$ channel function (2, 4). Indeed, a single mutation segregating in a given family can lead to conduction disease in some family members and Brugada syndrome in others (6, 7). What determines the ultimate phenotype — Brugada syndrome versus isolated conduction disease — is unknown. Sex, age, and genetic modifiers (e.g., common polymorphisms) have been proposed as modulators of the clinical phenotypes (5, 25, 26).

The reported effects of β1 on $Na_V1.5$ channels are controversial (32). Some groups have reported that β1 increases $Na_V1.5$ currents with or without affecting voltage dependence or channel kinetics, while others have reported no effect of β1 on $Na_V1.5$ current (20, 33–37). The β1B variant has to date only been studied in coexpression studies with the neuronal sodium channel $Na_V1.2$ (encoded by *SCN2A*), where it was shown to increase sodium current and cause a small negative shift in voltage dependence of activation (19). In our experiments, WT β1 and β1B had similar effects on $Na_V1.5$ current: both increased sodium currents and led to hyperpolarizing (negative) shifts in voltage dependence of activation and inactivation.

Not only were the effects of the WT β subunits on $Na_V1.5$ current similar, but the effects of the p.Glu87Gln mutation in the β1 background (p.Glu87Gln β1) were also similar to those in the β1B background (p.Glu87Gln β1B). Although the β1 and β1B variants share the same topology (an N-terminal extracellular immunoglobulin domain, a transmembrane domain, and a C-terminal cytoplasmic domain), their sequence identity is limited to the extracellular immunoglobulin domain; the C-terminal half of β1B, residues 150–268, has only approximately 17% amino acid sequence identity with β1 (19). Taken together, the data suggest that the molecular determinants of β1 and β1B modulation of $Na_V1.5$ cell-surface expression and gating likely reside in the extracellular immunoglobulin domain. This is in line with previous studies of skeletal muscle ($Na_V1.4$ encoded by *SCN4A*) and neuronal ($Na_V1.2$) sodium channel α subunits that have shown that deletion of the intracellular domain of the β1 subunit has no effect on its modulation of α subunit function, whereas deletions within the extracellular domain block modulation (38–40). Alternatively, specific residues may not be as important as preservation of overall structural motifs, as suggested by the data of Zimmer

and Benndorf, who reported that the β1 subunit modulates $Na_V1.5$ via the membrane anchor plus additional intracellular or extracellular regions (41).

In addition to modulation of sodium channel α subunit expression and function, other roles have been suggested for β subunits: these include acting as adhesion molecules or as participants in signal transduction (16, 32). The different transmembrane and C-terminal domains of β1 and β1B might therefore lead to participation in different signaling pathways. For instance, phosphorylation of the tyrosine at position 181 of the β1 C terminus regulates its interaction with ankyrin-G (42), which is thought to be critical for ankyrin-G localization within cardiomyocytes (intercalated discs versus T tubules). β1B lacks this tyrosine in its C-terminal domain, so a role for β1B as a modulator of this function seems less likely.

Another mechanism regulating function of β subunits is the potential for cleavage by β-site amyloid precursor protein–cleaving enzyme (BACE1) and γ-secretase, resulting in the release of the N- and C-terminal fragments (43). The processed C-terminal fragment of β2 and β4 has been reported to be associated with cell adhesion, migration, and morphogenesis in neuronal cells as well as regulation of the expression level of the neuronal sodium channel $Na_V1.1$ (44–46). Thus, p.Trp179X β1B may result in absence of functions depending on the generation of a β subunit C-terminal fragment by BACE1. However, a role for BACE1 cleavage has not been studied in either human β1 subunit or cardiomyocytes, and the cleavage site located at the common juxtamembrane domain in β1 and β1B is not conserved between human and mice (19, 43).

Mutations in *SCN1B* have been previously reported in generalized epilepsy with febrile seizures plus (47), and β1-null mice exhibit a severe seizure disorder and die at approximately 3 weeks of age (48). In addition, these mice exhibit bradycardia and prolonged rate-corrected QT intervals (27). These changes suggest that β1 plays an important role in the murine heart, although it is possible that the changes are a consequence of the severe overall developmental phenotype in this model (48). To our knowledge, defects in cardiac function have not been investigated in *SCN1B* mutation carriers presenting with epilepsy (32, 49). Conversely, we have observed no neurological phenotype in our patients. Four *SCN1B* mutations have been linked to epilepsy to date (47, 49, 50), all of which localize to the extracellular immunoglobulin-like fold of the protein, as does the p.Glu87Gln mutation reported here. One additional possible link between the cardiac and neurological phenotypes associated with β1 mutations is the syndrome of sudden unexpected death in epilepsy (SUDEP) (51), where a role for cardiac bradyarrhythmias has been proposed (52).

To date, *SCN5A* mutations are the most common cause identified in cases of Brugada syndrome, and *SCN5A* is the only identified causative gene in conduction disease (2, 11). However, *SCN5A* mutations are not identified in the majority of patients, and it has been reported that the frequency of mutations in other implicated genes (*CACNA1C*, *CACNB2b*, *GPD1L*) is also low in Brugada syndrome (12–14). In this study, *SCN1B* mutations were identified in less than 1% of probands with Brugada syndrome and less than 5% of probands with conduction disease and thus account for a small subset of these inherited arrhythmic syndromes.

A conventional heterologous mammalian expression system was used for functional assessment of the mutations. The environment in this approach is different from that in native cardiomyocytes, and other proteins known to associate with the sodium channel complex, such as other β subunits, are generally absent. Despite these limitations, the in vitro characteristics of the mutations were concordant with the phenotype observed in the patients, which, in combination with the genetic data presented, supports the hypothesis of a causal relationship between the mutations and disease.

In summary, we have for the first time to our knowledge identified *SCN1B* mutations in families with conduction disease and Brugada syndrome. We have shown expression of the β1 subunit transcript and the alternate β1B subunit transcript variant in human heart and demonstrated reduced $Na_V1.5$ sodium current as a result of loss or altered β subunit modulation of Nav1.5 current. These findings implicate *SCN1B* as a disease gene for human arrhythmia susceptibility.

Methods

Study populations. The study populations consisted of: (a) unrelated Brugada syndrome probands identified and characterized at the Academic Medical Center, Amsterdam (n = 38), l'institut du thorax, Nantes, (n = 216), and the Niigata University Graduate School of Medical and Dental Sciences (n = 28); and (b) patients with cardiac conduction disease were identified and characterized at the Academic Medical Center (n = 2), l'institut du thorax (n = 39), and Ege University School of Medicine (n = 3). The study was performed according to a protocol approved by the Medical Ethical Committee, Academic Medical Center, Amsterdam; Comité de Protection des Personnes, Nantes; Ege University Research Ethics Committee; and Medical Research Ethics Committee, Niigata University Graduate School of Medical and Dental Sciences. Informed consent was obtained from all patients. Coding region and splice site mutations in *SCN5A* had been previously excluded in all probands by single-strand confirmation polymorphism analysis, denaturing HPLC sequencing, or direct sequencing using primers in flanking intronic sequences.

Mutation analysis. Probands with Brugada syndrome and cardiac conduction disease were screened for mutations in regions of the *SCN1B* gene encoding β1 and β1B, except for Japanese probands, who were screened only in the regions of *SCN1B* gene encoding β1B. Screening for mutations was performed by PCR amplification of coding regions and flanking intronic sequences, followed by direct sequencing of amplicons on an ABI PRISM 3730 DNA Sequence Detection System (Applied Biosystems). Primer sequences are listed in Supplemental Table 2.

Control populations. We screened randomly selected and unrelated white Dutch individuals (n = 176); white individuals (n = 702) selected from the KORA S4 survey, which included population-based southern German individuals (n = 4,261) surveyed between 1999 and 2001 (53); unrelated white Turkish individuals (n = 150); and 4 different ethnic groups (white, African American, Hispanic, Asian; n = 94 for each group) from the Coriell Cell Repositories. The Coriell samples were resequenced as described above by the J. Craig Venter Institute through the NHLBI DNA Resequencing and Genotyping Program. The other control samples were genotyped at the identified mutation sites.

Subunit mRNA abundances in human cardiac tissue. Real-time RT-PCR was used to quantify subunit abundances. Assays were conducted in nondiseased human hearts obtained from the University of Szeged, Szeged, Hungary, that were technically unusable for transplantation based on logistic considerations (54). Before cardiac explantation, organ donor patients did not receive medication except dobutamine, furosemide, and plasma expanders. The investigations conformed to the principles outlined in the Helsinki Declaration of the World Medical Association. All experimental protocols were approved by the Ethical Review Board of the Medical Center of the University of Szeged (no. 51-57/1997 OEJ). The left ventricles from 6 donors and the right ventricles from 6 donors were dissected and stored in cardioplegic solution at 4°C for approximately 4–8 hours before being

frozen in liquid nitrogen. Purkinje fiber mRNA was extracted from false tendons dissected from the ventricles of 6 donors. Further information on the donors is presented in Supplemental Table 3.

Total RNA from each cardiac sample was isolated and DNase treated with the RNeasy Fibrous Tissue Mini Kit (QIAGEN) following the manufacturer's instructions. The quality of total RNA was assessed with PAGE (2100 Bioanalyzer; Agilent Technologies). Absence of genomic DNA contamination was verified by PCR. First-strand cDNA was synthesized from 2 μg total RNA with High-Capacity cDNA Archive Kit (Applied Biosystems). Real-time PCR was performed on a TaqMan system with predesigned 6-carboxyfluorescein–labeled (FAM-labeled) fluorogenic TaqMan probe and primers for β1, custom-designed TaqMan probe and primers for β1B (located in the retained segment of intron 3), and 1× TaqMan Universal PCR Master Mix (Applied Biosystems). PCR efficiency of the β1 and β1B fluorescent probes was estimated at approximately 98%. After 2 minutes at 50°C and 10 minutes at 95°C, 40 cycles of amplification were performed with the ABI PRISM 7900HT Sequence Detection System (Applied Biosystems). Data were collected with instrument spectral compensation by Applied Biosystems SDS 2.1 software and analyzed with the Ct relative quantification method (55). Fluorescence signals were normalized to the housekeeping gene hypoxanthine phosphoribosyl transferase 1 (*HPRT1*). For each sample, β1 and β1B transcripts were quantified in duplicate. The values were averaged and then used for the $2^{-\Delta Ct} \times 100$ calculation, where $2^{-\Delta Ct}$ corresponds to expression relative to *HPRT*. Primer and probe sequences are listed in Supplemental Table 4.

Generation of expression vectors. Full-length human β1 cDNA (GenBank accession number NM_001037) subcloned into a bicistronic vector also carrying the cDNA for enhanced eGFP (pEGFP-IRES; BD Biosciences – Clontech) was supplied by Alfred George Jr. (Vanderbilt University, Nashville, Tennessee, USA). Full-length human β1B cDNA (GenBank accession number NM_199037) was cloned from human ventricular mRNA, supplied by Katherine Murray (Vanderbilt University). The β1B cDNA was subcloned into a pEGFP-IRES vector (BD Biosciences – Clontech). Mutant constructs were prepared using the QuikChange II XL Site-Directed Mutagenesis Kit (Stratagene) according to the manufacturer's instructions. The inserts were subsequently sequenced to ensure that there was no other mutation besides the intended one.

Transient transfection in CHO cells. For functional analysis, cultured CHO cells were transiently transfected with the constructs described above using FuGENE 6 (Roche Applied Science). Constructs encoding β1 or β1B subunits (1 μg, unless otherwise specified) were cotransfected with the pBK-CMV vector (1 μg; Stratagene) encoding *SCN5A* (GenBank accession number NM_000335), supplied by Alfred George Jr. To study dominant negative effects, mutant β1 or β1B construct (0.5 μg or 1 μg) was cotransfected with the same amount of construct for WT β1 or β1B subunit that had been subcloned into a bicistronic vector also carrying cDNA for red fluorescent protein from *Discosoma* version T3 (pDsRed-IRES; supplied by Alfred George Jr.) along with *SCN5A* (1 μg). When *SCN5A* was transfected without β subunits, the plasmid encoding the eGFP (pEGFP-IRES; BD Biosciences – Clontech) with no β subunit insert was cotransfected. Cells were grown for 48 hours after transfection before study.

Electrophysiology. Cells displaying green fluorescence were chosen for study; in experiments with transfection of both WT and mutant β subunits, cells displaying both green and red fluorescence were chosen. Sodium currents were measured at room temperature using the whole-cell configuration of the patch-clamp technique with an Axopatch 200B amplifier (Molecular Devices). The extracellular bath solution contained (in mmol/l): 145 NaCl, 4.0 KCl, 1.0 $MgCl_2$, 1.8 $CaCl_2$, 10 glucose, 10 HEPES, pH 7.4 (NaOH). Patch pipettes (~1.5 MΩ) contained (in mmol/l): 10 NaF, 110 CsF, 20 CsCl, 10 EGTA, and 10 HEPES, pH 7.4 (CsOH). Currents were filtered at 5 kHz and digitized at 50 kHz. Cell capacitance and series resistance were compensated for by at least 80%. Voltage control, data acquisition, and analysis were accomplished using pCLAMP 9.2 and Clampfit 9.2 software (Molecular Devices).

Sodium current properties were determined by voltage clamp protocols as shown in the relevant figures. Cells were held at −120 mV, and currents were elicited with 50-ms depolarizing pulses from −80 to 60 mV in 10-mV increments. Voltage dependence of inactivation was studied using 500-ms prepulses from −120 to −20 mV in 10-mV increments, followed by a test pulse to −20 mV. The rate of recovery from inactivation was examined by 50-ms conditioning pulse to −20 mV from a holding potential of −120 mV, followed by a varying recovery duration and a 10-ms test pulse to −20 mV. All currents were normalized to cell capacitance. The voltage dependence of sodium current was determined by fitting a Boltzmann function ($y = [1 + \exp\{(V - V_{1/2}) / k\}]^{-1}$), yielding the voltage required to achieve half-maximal conductance or channel availability ($V_{1/2}$) and slope factor (k). The time constants of recovery from inactivation were determined using a double-exponential function ($y = A_f\{1 - \exp(-t / \tau_f)\} + A_s\{1 - \exp(-t / \tau_s)\}$), where τ_f and τ_s are the time constants of fast and slow components, and A_f and A_s are the fractions of the fast and slow components.

Statistics. Electrophysiological data are expressed as mean ± SEM. Gene expression data are expressed as median ± median absolute deviation. All statistical analyses were conducted with SPSS version 12.0. To test for significant differences among groups, an unpaired 2-tailed t test or ANOVA was used. The level of statistical significance was $P < 0.05$.

Acknowledgments

We thank Leander Beekman, Peter van Tintelen, Arie O. Verkerk, Carol Ann Remme, Alfred George Jr., Katherine Murray, Sabina Kupershmidt, Kai Liu, Sameer Chopra, Nathalie Gaborit, Satoru Komura, Mahmut Akyol, and Moritz Sinner for their contributions to performing and/or analyzing this work and for helpful discussions. This work was supported by grants from the NIH (HL46681 and HL65962 to D.M. Roden), a Fondation Leducq Trans-Atlantic Network of Excellence grant (05 CVD 01, Preventing Sudden Death, to D. Escande, J.-J. Schott, A.M. Wilde, S. Kääb, and D.M. Roden), Netherlands Heart Foundation grant 2003T302 (to A.A.M. Wilde), the Interuniversity Cardiology Institute of The Netherlands (project 27, to A.A.M. Wilde), Agence Nationale de la Recherche grant 05-MRAR-028 (to J.-J. Schott), Agence Nationale de la Recherche grants 05-MRAR-028 and 06-MRAR-022 (to J.-J. Schott), German Federal Ministry of Education and Research (BMBF) grants 01GI0204, 01GS0499, 01GI0204, and 01GR0103 (to S. Kääb, A. Pfeufer, and H.-E. Wichmann), and a Sumitomo Life Social Foundation grant (to H. Watanabe). The KORA platform is funded by the BMBF and by the State of Bavaria. Resequencing of Coriell samples was performed by the J. Craig Venter Institute through the NHLBI Resequencing and Genotyping Program. We also thank Andras Varro (University of Szeged) for providing the human tissues. C.R. Bezzina is an Established Investigator of The Netherlands Heart Foundation (grant 2005/T024).

Received for publication September 11, 2007, and accepted in revised form March 19, 2008.

Address correspondence to: Connie R. Bezzina, Heart Failure Research Center, Department of Experimental Cardiology, L2-108-1, Meibergdreef 15, 1105 AZ Amsterdam, The Netherlands. Phone: 31-20-5665403; Fax: 31-20-6976177; E-mail: C.R.Bezzina@amc.uva.nl.

Hiroshi Watanabe, Tamara T. Koopmann, and Solena Le Scouarnec contributed equally to this work.

1. Wang, Q., et al. 1995. SCN5A mutations associated with an inherited cardiac arrhythmia, long QT syndrome. *Cell.* **80**:805–811.
2. Schott, J.J., et al. 1999. Cardiac conduction defects associate with mutations in SCN5A. *Nat. Genet.* **23**:20–21.
3. Tan, H.L., et al. 2001. A sodium-channel mutation causes isolated cardiac conduction disease. *Nature.* **409**:1043–1047.
4. Chen, Q., et al. 1998. Genetic basis and molecular mechanism for idiopathic ventricular fibrillation. *Nature.* **392**:293–296.
5. Tan, H.L., Bezzina, C.R., Smits, J.P., Verkerk, A.O., and Wilde, A.A. 2003. Genetic control of sodium channel function. *Cardiovasc. Res.* **57**:961–973.
6. Bezzina, C., et al. 1999. A single Na(+) channel mutation causing both long-QT and Brugada syndromes. *Circ. Res.* **85**:1206–1213.
7. Kyndt, F., et al. 2001. Novel SCN5A mutation leading either to isolated cardiac conduction defect or Brugada syndrome in a large French family. *Circulation.* **104**:3081–3086.
8. Grant, A.O., et al. 2002. Long QT syndrome, Brugada syndrome, and conduction system disease are linked to a single sodium channel mutation. *J. Clin. Invest.* **110**:1201–1209.
9. Valdivia, C.R., et al. 2002. A novel SCN5A arrhythmia mutation, M1766L, with expression defect rescued by mexiletine. *Cardiovasc. Res.* **55**:279–289.
10. Remme, C.A., et al. 2006. Overlap syndrome of cardiac sodium channel disease in mice carrying the equivalent mutation of human SCN5A-1795insD. *Circulation.* **114**:2584–2594.
11. Shimizu, W., Aiba, T., and Kamakura, S. 2005. Mechanisms of disease: current understanding and future challenges in Brugada syndrome. *Nat. Clin. Pract. Cardiovasc. Med.* **2**:408–414.
12. London, B., et al. 2007. Mutation in glycerol-3-phosphate dehydrogenase 1 like gene (GPD1-L) decreases cardiac Na+ current and causes inherited arrhythmias. *Circulation.* **116**:2260–2268.
13. Koopmann, T.T., et al. 2007. Exclusion of multiple candidate genes and large genomic rearrangements in SCN5A in a Dutch Brugada syndrome cohort. *Heart Rhythm.* **4**:752–755.
14. Antzelevitch, C., et al. 2007. Loss-of-function mutations in the cardiac calcium channel underlie a new clinical entity characterized by ST-Segment elevation, short QT intervals, and sudden cardiac death. *Circulation.* **15**:442–449.
15. Moric, E., et al. 2003. The implications of genetic mutations in the sodium channel gene (SCN5A). *Europace.* **5**:325–334.
16. Isom, L.L. 2001. Sodium channel beta subunits: anything but auxiliary. *Neuroscientist.* **7**:42–54.
17. Abriel, H., and Kass, R.S. 2005. Regulation of the voltage-gated cardiac sodium channel Nav1.5 by interacting proteins. *Trends Cardiovasc. Med.* **15**:35–40.
18. Kazen-Gillespie, K.A., et al. 2000. Cloning, localization, and functional expression of sodium channel beta1A subunits. *J. Biol. Chem.* **275**:1079–1088.
19. Qin, N., et al. 2003. Molecular cloning and functional expression of the human sodium channel beta1B subunit, a novel splicing variant of the beta1 subunit. *Eur. J. Biochem.* **270**:4762–4770.
20. Nuss, H.B., et al. 1995. Functional association of the beta 1 subunit with human cardiac (hH1) and rat skeletal muscle (mu 1) sodium channel alpha subunits expressed in Xenopus oocytes. *J. Gen. Physiol.* **106**:1171–1191.
21. Wilde, A.A., et al. 2002. Proposed diagnostic criteria for the Brugada syndrome: consensus report. *Circulation.* **106**:2514–2519.
22. Dickinson, D.F. 2005. The normal ECG in childhood and adolescence. *Heart.* **91**:1626–1630.
23. Priori, S.G., Napolitano, C., and Schwartz, P.J. 1999. Low penetrance in the long-QT syndrome: clinical impact. *Circulation.* **99**:529–533.
24. Priori, S.G., et al. 2000. Clinical and genetic heterogeneity of right bundle branch block and ST-segment elevation syndrome: a prospective evaluation of 52 families. *Circulation.* **102**:2509–2515.
25. Viswanathan, P.C., Benson, D.W., and Balser, J.R. 2003. A common SCN5A polymorphism modulates the biophysical effects of an SCN5A mutation. *J. Clin. Invest.* **111**:341–346.
26. Bezzina, C.R., et al. 2006. Common sodium channel promoter haplotype in Asian subjects underlies variability in cardiac conduction. *Circulation.* **113**:338–344.
27. Lopez-Santiago, L.F., et al. 2007. Sodium channel Scn1b null mice exhibit prolonged QT and RR intervals. *J. Mol. Cell. Cardiol.* **43**:636–647.
28. Meregalli, P.G., Wilde, A.A., and Tan, H.L. 2005. Pathophysiological mechanisms of Brugada syndrome: depolarization disorder, repolarization disorder, or more? *Cardiovasc. Res.* **67**:367–378.
29. Baroudi, G., et al. 2001. Novel mechanism for Brugada syndrome: defective surface localization of an SCN5A mutant (R1432G). *Circ. Res.* **88**:e78–e83.
30. Yan, G.X., and Antzelevitch, C. 1999. Cellular basis for the Brugada syndrome and other mechanisms of arrhythmogenesis associated with ST-segment elevation. *Circulation.* **100**:1660–1666.
31. Antzelevitch, C., et al. 2005. Brugada syndrome: report of the second consensus conference: endorsed by the Heart Rhythm Society and the European Heart Rhythm Association. *Circulation.* **111**:659–670.
32. Meadows, L.S., and Isom, L.L. 2005. Sodium channels as macromolecular complexes: implications for inherited arrhythmia syndromes. *Cardiovasc. Res.* **67**:448–458.
33. Qu, Y., et al. 1995. Modulation of cardiac Na+ channel expression in Xenopus oocytes by beta 1 subunits. *J. Biol. Chem.* **270**:25696–25701.
34. Ko, S.H., Lenkowski, P.W., Lee, H.C., Mounsey, J.P., and Patel, M.K. 2005. Modulation of Na(v)1.5 by beta1- and beta3-subunit co-expression in mammalian cells. *Pflugers Arch.* **449**:403–412.
35. Johnson, D., Montpetit, M.L., Stocker, P.J., and Bennett, E.S. 2004. The sialic acid component of the beta1 subunit modulates voltage-gated sodium channel function. *J. Biol. Chem.* **279**:44303–44310.
36. Fahmi, A.I., et al. 2001. The sodium channel beta-subunit SCN3b modulates the kinetics of SCN5a and is expressed heterogeneously in sheep heart. *J. Physiol.* **537**:693–700.
37. Makita, N., Bennett, P.B., Jr., and George, A.L., Jr. 1994. Voltage-gated Na+ channel beta 1 subunit mRNA expressed in adult human skeletal muscle, heart, and brain is encoded by a single gene. *J. Biol. Chem.* **269**:7571–7578.
38. Chen, C., and Cannon, S.C. 1995. Modulation of Na+ channel inactivation by the beta 1 subunit: a deletion analysis. *Pflugers Arch.* **431**:186–195.
39. McCormick, K.A., et al. 1998. Molecular determinants of Na+ channel function in the extracellular domain of the beta1 subunit. *J. Biol. Chem.* **273**:3954–3962.
40. McCormick, K.A., Srinivasan, J., White, K., Scheuer, T., and Catterall, W.A. 1999. The extracellular domain of the beta1 subunit is both necessary and sufficient for beta1-like modulation of sodium channel gating. *J. Biol. Chem.* **274**:32638–32646.
41. Zimmer, T., and Benndorf, K. 2002. The human heart and rat brain IIA Na+ channels interact with different molecular regions of the beta1 subunit. *J. Gen. Physiol.* **120**:887–895.
42. Malhotra, J.D., Thyagarajan, V., Chen, C., and Isom, L.L. 2004. Tyrosine-phosphorylated and nonphosphorylated sodium channel beta1 subunits are differentially localized in cardiac myocytes. *J. Biol. Chem.* **279**:40748–40754.
43. Wong, H.K., et al. 2005. beta Subunits of voltage-gated sodium channels are novel substrates of beta-site amyloid precursor protein-cleaving enzyme (BACE1) and gamma-secretase. *J. Biol. Chem.* **280**:23009–23017.
44. Kim, D.Y., Ingano, L.A., Carey, B.W., Pettingell, W.H., and Kovacs, D.M. 2005. Presenilin/gamma-secretase-mediated cleavage of the voltage-gated sodium channel beta2-subunit regulates cell adhesion and migration. *J. Biol. Chem.* **280**:23251–23261.
45. Kim, D.Y., et al. 2007. BACE1 regulates voltage-gated sodium channels and neuronal activity. *Nat. Cell Biol.* **9**:755–764.
46. Miyazaki, H., et al. 2007. BACE1 modulates filopodia-like protrusions induced by sodium channel beta4 subunit. *Biochem. Biophys. Res. Commun.* **361**:43–48.
47. Wallace, R.H., et al. 1998. Febrile seizures and generalized epilepsy associated with a mutation in the Na+-channel beta1 subunit gene SCN1B. *Nat. Genet.* **19**:366–370.
48. Chen, C., et al. 2004. Mice lacking sodium channel beta1 subunits display defects in neuronal excitability, sodium channel expression, and nodal architecture. *J. Neurosci.* **24**:4030–4042.
49. Scheffer, I.E., et al. 2007. Temporal lobe epilepsy and GEFS+ phenotypes associated with SCN1B mutations. *Brain.* **130**:100–109.
50. Audenaert, D., et al. 2003. A deletion in SCN1B is associated with febrile seizures and early-onset absence epilepsy. *Neurology.* **61**:854–856.
51. Nashef, L., Hindocha, N., and Makoff, A. 2007. Risk factors in sudden death in epilepsy (SUDEP): the quest for mechanisms. *Epilepsia.* **48**:859–871.
52. Rugg-Gunn, F.J., Simister, R.J., Squirrell, M., Holdright, D.R., and Duncan, J.S. 2004. Cardiac arrhythmias in focal epilepsy: a prospective long-term study. *Lancet.* **364**:2212–2219.
53. Wichmann, H.E., Gieger, C., and Illig, T. 2005. KORA-gen—resource for population genetics, controls and a broad spectrum of disease phenotypes. *Gesundheitswesen.* **67**(Suppl. 1):S26–S30.
54. Gaborit, N., Le Bouter, S., Szuts, V., Varro, A., Escande, D., Nattel, S., and Demolombe, S. 2007. Regional and tissue specific transcript signatures of ion channel genes in the non-diseased human heart. *J. Physiol.* **582**:675–693.
55. Livak, K.J., and Schmittgen, T.D. 2001. Analysis of relative gene expression data using real-time quantitative PCR and the 2(-Delta Delta C(T)) Method. *Methods.* **25**:402–408.

Journal of the American College of Cardiology
© 2008 by the American College of Cardiology Foundation
Published by Elsevier Inc.

Vol. 51, No. 12, 2008
ISSN 0735-1097/08/$34.00
doi:10.1016/j.jacc.2007.10.060

Atrial Fibrillation in Patients With Brugada Syndrome

Relationships of Gene Mutation, Electrophysiology, and Clinical Backgrounds

Kengo F. Kusano, MD, Makiko Taniyama, MD, Kazufumi Nakamura, MD, Daiji Miura, PHD, Kimikazu Banba, MD, Satoshi Nagase, MD, Hiroshi Morita, MD, Nobuhiro Nishii, MD, Atsuyuki Watanabe, MD, Takeshi Tada, MD, Masato Murakami, MD, Kohei Miyaji, MD, Shigeki Hiramatsu, MD, Koji Nakagawa, MD, Masamichi Tanaka, MD, Aya Miura, MD, Hideo Kimura, MD, Soichiro Fuke, MD, Wakako Sumita, MD, Satoru Sakuragi, MD, Shigemi Urakawa, MD, Jun Iwasaki, MD, Tohru Ohe, MD, FACC

Okayama, Japan

Objectives The goal of our work was to examine the relationships of atrial fibrillation (AF) with genetic, clinical, and electrophysiological backgrounds in Brugada syndrome (BrS).

Background Atrial fibrillation is often observed in patients with BrS and indicates that electrical abnormality might exist in the atrium as well as in the ventricle. *SCN5A*, a gene encoding the cardiac sodium channel, has been reported to be causally related to BrS. However, little is known about the relationships of atrial arrhythmias with genetic, clinical, and electrophysiological backgrounds of BrS.

Methods Seventy-three BrS patients (49 ± 12 years of age, men/women = 72/1) were studied. The existence of *SCN5A* mutation and clinical variables (syncopal episode, documented ventricular fibrillation [VF], and family history of sudden death) were compared with spontaneous AF episodes. Genetic and clinical variables were also compared with electrophysiologic (EP) parameters: atrial refractory period, interatrial conduction time (CT), repetitive atrial firing, and AF induction by atrial extra-stimulus testing.

Results Spontaneous AF occurred in 10 (13.7%) of the BrS patients and *SCN5A* mutation was detected in 15 patients. Spontaneous AF was associated with higher incidence of syncopal episodes (60.0% vs. 22.2%, $p < 0.03$) and documented VF (40.0% vs. 14.3%, $p < 0.05$). *SCN5A* mutation was associated with prolonged CT ($p < 0.03$) and AF induction ($p < 0.05$) in EP study, but not related to the spontaneous AF episode and other clinical variables. In patients with documented VF, higher incidence of spontaneous AF (30.8% vs. 10.0%, $p < 0.05$), AF induction (53.8% vs. 20.0%, $p < 0.03$), and prolonged CT was observed.

Conclusions Spontaneous AF and VF are closely linked clinically and electrophysiologically in BrS patients. Patients with spontaneous AF have more severe clinical backgrounds in BrS. *SCN5A* mutation is associated with electrical abnormality but not disease severity. (J Am Coll Cardiol 2008;51:1169–75) © 2008 by the American College of Cardiology Foundation

Brugada syndrome (BrS) is a distinct form of idiopathic ventricular fibrillation (VF) characterized by a unique electrographic (ECG) pattern consisting of a right bundle branch block-like morphology and ST-segment elevation in precordial leads (1–3). In addition to the ventricular arrhythmias, atrial arrhythmias are also often observed in this syndrome (4–6), indicating that electrical abnormality might exist in the atrium as well as in the ventricle. We, therefore, speculated that patients with BrS and spontaneous atrial fibrillation (AF) have more advanced disease process.

See page 1176

The human cardiac sodium channel (*SCN5A*) is responsible for the fast depolarization upstroke for the cardiac action potential (7). Mutations in *SCN5A* have been previ-

From the Department of Cardiovascular Medicine, Okayama University Graduate School of Medicine, Dentistry and Pharmaceutical Sciences, Okayama, Japan. This work was supported, in part, by Grant-in-Aid for Scientific Research (No. 18790501), Grant-in-Aid for Young Scientists (No. 17689026) from the Ministry of Education, Culture, Sports, Science and Technology, Japan and Health Sciences Research grants (H18-Research on Human Genome-002) from the Ministry of Health, Labor and Welfare, Japan. This work was also supported, in part, by a grant from the Japan Foundation of Cardiovascular Research, Tokyo, Japan. Drs. Kusano and Taniyama contributed equally to this study.

Manuscript received September 19, 2007; accepted October 19, 2007.

JACC Vol. 51, No. 12. 2008
March 25, 2008:1169–75

Abbreviations and Acronyms

AF = atrial fibrillation
BrS = Brugada syndrome
CS = coronary sinus
CT = conduction time
EP = electrophysiology/electrophysiological
ERP = effective refractory period
FH = family history of sudden death
ICD = implantable cardioverter-defibrillator
PCR = polymerase chain reaction
RAA = right atrial appendage
RAF = repetitive atrial firing
SCN5A = pore-forming region of the human cardiac sodium channel
VF = ventricular fibrillation

ously discovered in a wide spectrum of cardiac rhythm disorders: the long QT syndrome (8), BrS (7), sick sinus syndrome (9,10), cardiac conduction defect (11), and AF (12). In patients with BrS, *SCN5A* mutations have been reported to be causally linked to familial BrS (7,13). However, little is known about the relationships of atrial arrhythmias with genetic, clinical, and electrophysiological (EP) backgrounds. We, therefore, examined the relationships between genetic, EP, and clinical variables to AF in BrS patients.

Methods

Patient population and clinical data collection. Patients diagnosed with BrS in our hospital between 1997 to 2006 were studied. All of the tests that were performed were approved by the medical ethical review committees of our hospital. Informed consent was obtained from all patients. Clinical data, including data on age at diagnosis, gender, family history, documented VF, syncopal episodes, and implantable cardioverter-defibrillator (ICD) implantation, were obtained from patient records. Family history of sudden death (FH) was defined as unknown sudden death at less than the age of 50 years. All patients showed a typical ECG "Brugada pattern," which was defined previously (1). If the standard ECG pattern showed a type 2 or 3 Brugada pattern, 1 mg/kg of pilsicainide (a pure sodium channel blocker) was intravenously administered for 10 min with continuous monitoring in the intensive care unit and it was confirmed that the Brugada pattern had changed to a type 1 pattern.

Evaluation of incidence of AF. The occurrence of spontaneous AF was evaluated by clinical follow-up (every month), in which the patient's symptoms were observed and 24-h Holter recordings without any drugs were performed. Continuous ECG monitoring was also performed for 2 to 3 weeks during admission.

Analysis of *SCN5A* mutation. This study was performed in compliance with guidelines for human genome studies of the Ethics Committee of Okayama University. Informed consent was obtained from all patients. All exons of SCN5A were amplified by polymerase chain reaction (PCR) from deoxyribonucleic acid (DNA) isolated from peripheral leukocytes of the patients. Genomic DNA was extracted from peripheral blood leucocytes using a DNA extraction kit (Gentra, Minneapolis, Minnesota) and was stored at −30°C until use.

Twenty-seven exons of the *SCN5A* gene were amplified with previously reported intronic primers (14). *SCN5A* gene exon 1 is a noncoding region, and this region was not analyzed in this study. Exons 6, 17-1 Sense, 21, and 25 were not able to be amplified sufficiently by the primers, and we designed new intronic primers. The following primers were used in this study: 5′-GTT ATC CCA GGT AAG ATG CCC-3′ (sense) and 5′-TGG TGA CAG GCA CAT TCG AAG-3′ (antisense) for exon 6, 5′-AAG CCT CGG AGC TGT TTG TCA CA-3′ (sense) for exon 17-1, 5′-TGC CTG GTG CAG GGT GGA AT-3′ (sense) and 5′-ACT CAG ACT TAC GTC CTC CTT C-3′ (antisense) for exon 21, and 5′-TCT TTC CCA CAG AAT GGA CAC C-3′ (sense) and 5′-AAG GTG AGA TGG GAC CTG GAG-3′ (antisense) for exon 25. Polymerase chain reaction was performed in 25-μl reaction volumes containing 50 ng of genomic DNA, 20 pmol of each primer, 0.8 mM dNTPs, 1 X reaction buffer, 1.5 mM $MgCl_2$, and 0.7 U of AmpliTaq Gold DNA polymerase (Applied Biosystems, Foster City, California) or TAKARA Taq (Takara Bio Inc., Otsu, Shiga, Japan). All PCR products were purified with a PCR products pre-sequencing kit (Amersham Life Science, Buckinghamshire, United Kingdom), reacted with a Big Dye Terminator FS ready-reaction kit (Applied Biosystems), and analyzed on an ABI PRISM3130xl sequencer (Applied Biosystems). Mutations were analyzed at least 3 times by independent PCR amplification and sequencing. Polymerase chain reaction products were subjected to single-strand conformation polymorphism analysis followed by direct sequence analysis.

EP study. After obtaining written informed consent from patients, an EP study was performed as described previously (6,15,16) in all patients. In brief, after right femoral and right jugular venous access had been obtained, 3 quadripolar electrode catheters (6-F) with an interelectrode distance of 5 mm (EP Technologies, Boston Scientific, Inc., Sunnyvale, California) were positioned in the right atrial appendage (RAA), His bundle region, and right ventricle, and an octopolar catheter (6-F) with an interelectrode distance of 2.5 mm (EP Technologies, Boston Scientific, Inc.) was positioned in the coronary sinus (CS). To reduce the differences among patients, the proximal electrode of CS catheter was positioned at the CS ostium and the distal electrode was located at the lateral wall of the left atrium in all patients. An extra-stimulus (S2) was delivered after 8 beats of drive pacing (S1) at a basic cycle length of 600 ms. The S1-S2 interval was decreased in 10-ms steps until the effective refractory period (ERP) of the RAA was reached. Sinus node recovery time was also measured during the EP study.

The parameters during EP study were as follows: 1) ERP of the RAA by atrial extra-stimulus testing; 2) interatrial conduction time (CT) measured by CT from the stimulus at the right atrium to atrial deflection at the distal portion of the CS; 3) the duration of local atrial electrogram (A) recorded at atrial pacing site; 4) repetitive atrial firing (RAF)